Transportation Research Part B 137 (2020) 133–153

Contents lists available at ScienceDirect

Transportation Research Part B

journal homepage: www.elsevier.com/locate/trb

Adaptive perimeter control for multi-region accumulation-based models with state delays

Jack Haddad*, Zhengfei Zheng

Technion-Israel Institute of Technology, Faculty of Civil and Environmental Engineering, Technion Sustainable Mobility and Robust Transportation (T-SMART) Laboratory, Israel

ARTICLE INFO

Article history:
Received 6 April 2018
Accepted 25 May 2018
Available online 14 July 2018

Keywords:
Accumulation-based models
Macroscopic fundamental diagram
State delay
Adaptive perimeter control

ABSTRACT

Enhancing macroscopic fundamental diagram (MFD) dynamic models and improving perimeter control algorithms are the current main research challenges in the MFD research area. Over the last decade, different accumulation-based dynamic models, describing the traffic flow dynamics of one or multi-region systems, have been developed in different forms relying on vehicle conservation equations.

In this research, two enhanced accumulation-based models are developed by incorporating into model structure the time-delay (time-lag) effects as an important factor. The first model incorporates state delay in the MFD output to improve the dynamics, to better represent wave propagation and travel time evolution within the region, especially when the change in demand is fast. While in the second model delayed interconnections are introduced in the dynamic equations to model data processing and communication delays between interconnected regions. The two linearized models are formulated in interconnected forms. Then, the reference model adaptive control approach has been implemented to allow us designing distributed adaptive perimeter control laws. The developed adaptive control scheme postulates one controller structure, however, the controllers' gains vary with time to adapt themselves against the model parameter uncertainties and state delays. The numerical results demonstrate the flexibility of the distributed adaptive perimeter controllers in handling different cases and various traffic situations with state delays.

1. Introduction

Intensive research works have founded the idea of modeling and perimeter control of traffic flow on large-scale networks with macroscopic fundamental diagrams (MFDs), e.g. (Godfrey, 1969; Daganzo, 2007; Geroliminis and Daganzo, 2008; Geroliminis et al., 2013; Haddad and Geroliminis, 2012; Geroliminis and Sun, 2011b; Buisson and Ladier, 2009; Ji et al., 2010; Mazloumian et al., 2010; Daganzo et al., 2011; Gayah and Daganzo, 2011; Zhang et al., 2013; Mahmassani et al., 1987; Olszewski et al., 1995; Knoop et al., 2012; Mahmassani et al., 2013; Keyvan-Ekbatani et al., 2013; Leclercq et al., 2014; Ortigosa et al., 2014), and others. Large-scale traffic control problems have been approached with model-based control methods, utilizing aggregate MFD-based models. Enhancing MFD dynamic models and improving perimeter control algorithms are the current main research challenges in the MFD research area. Recent research efforts have been devoted to these tasks, e.g.

* Corresponding author.
E-mail address: jh@technion.ac.il (J. Haddad).

https://doi.org/10.1016/j.trb.2018.05.019
0191-2615/

(Leclercq et al., 2015; Laval and Castrillón, 2015; Haddad, 2015; Ramezani et al., 2015; Mahmassani et al., 2013; Keyvan-Ekbatani et al., 2015; Haddad and Mirkin, 2016b; Lamotte and Geroliminis, 2016; Mariotte et al., 2017).

The hysteresis phenomena and heterogeneity of urban regions challenge the dynamic modeling task based on MFD (Daganzo et al., 2011; Buisson and Ladier, 2009; Saberi and Mahmassani, 2012; Geroliminis and Sun, 2011a; Ramezani et al., 2015). The heterogeneous networks might not have a well-defined MFD, especially in the decreasing part. Partitioning such a network into homogenous regions can result in well-defined shape MFD with low scatter, as shown in Ji and Geroliminis (2012). In order to deal with scattered MFD (not well-defined) in case of heterogeneity, and/or well-defined shape of MFD but not defined explicitly in advance in case of partitioning, one can integrate parameter uncertainties in the model to cope with such difficulties. In Haddad and Shraiber (2014); Haddad (2015), robust perimeter controllers have been designed to systematically take into account uncertainties in MFD-based dynamics. In Haddad and Shraiber (2014), considering a single region control problem, a robust fixed structure perimeter controller was designed with the help of quantitative feedback theory, based on a partially uncertain (interval) MFD. That is, the relevant function that approximates the aggregate relationship between traffic variables is an interval function that might change within specified bounds. Fig. 4 provides a shape of such partially uncertain (interval) MFD, where the red curve corresponds to the nominal MFD. Haddad (2015) considers modeling and control of uncertain MFD systems for multi-region networks. The uncertain MFD model is utilized to design a robust feedback controller by the Interpolation Control approach.

Over the last few years, the above-mentioned studies of MFD modeling and perimeter control were inspired by the original basic *accumulation-based* model of Daganzo (2007), which was developed further for two regions in Geroliminis et al. (2013). Different accumulation-based dynamic models, describing the traffic flow dynamics of one or multi-region systems, have been developed in different forms relying on vehicle conservation equations. Some of these models are based on total vehicles in the region, e.g. in Aboudolas and Geroliminis (2013); Haddad (2015), while other works decomposed the vehicle trips based on their destinations, e.g. in Geroliminis et al. (2013); Haddad and Mirkin (2017), resulting in accumulation states based on destinations.

Note that in accumulation-based models, as already stated in Daganzo (2007), it is assumed that: (i) the system demand evolves slowly over time, and (ii) the average vehicle trip length is the same for all origins, implying a proportional relationship between outflow and production. The validity and the effect of relaxing these assumptions were recently investigated and analyzed in Leclercq et al. (2015); Yildirimoglu and Geroliminis (2014); Mariotte et al. (2017). It was demonstrated in Mariotte et al. (2017), via several examples for *a single region system*, that the accumulation-based model is more suitable for slow-varying demand situations. The MFD outflow may overreact to a sudden demand change leading "to inconsistent propagation of information between opposite perimeter boundaries". Vehicles enter an urban region at time t, they are expected to travel at average speed determined by the accumulation, and will exit the network only after some time delays, equal to the needed travel times to travel their trip lengths.

Recently, *trip-based* MFD models were formulated to consider variable trip lengths in single-region dynamics in Arnott (2013); Fosgerau (2015); Lamotte and Geroliminis (2016); Mariotte et al. (2017). The major insight of the analytical investigation in Mariotte et al. (2017), which was also stated in Kouvelas et al. (2017); Haddad (2017), is that the accumulation-based model has no memory while the trip-based approach accounts for a reaction time. Compared with the current state-of-the-art for accumulation-based models, the trip-based approach appears to better represent wave propagation and travel time evolution within the region, when the change in demand is fast, as demonstrated in Mariotte et al. (2017). However, designing perimeter control for multi-region systems with trip-based models, instead of accumulation-based models, would challenge the control design task. This issue should be investigated in the near future, hopefully, after developing the trip-based models for multi-region systems. However, in this paper, we aim at enhancing the accumulation-based model by incorporating time delays, and based on the enhanced model to develop new adaptive perimeter control schemes. Hence, the main contributions of the current paper are summarized as follows: (1) time delays are incorporated into the dynamics to enhance the accumulation-based models, and (2) new adaptive perimeter control schemes are implemented for the MFD control problems. The present paper follows the structure of coordinated distributed perimeter controllers for uncertain large-scale urban road networks, which was recently presented in Haddad and Mirkin (2017). The coordinated distributed control structure, shown in Fig. 3, is used for the control design, where an upper control level, i.e. coordinator or the large-scale traffic management center, coordinates the functioning of the local perimeter controllers by providing also the reference signals of the other urban regions, so called model co-ordination. In such a structure the perimeter controllers can operate independently from each other, i.e. each local perimeter controller may on-line measure only a subset the variables of the network. More information related the distributed control structure is presented in Section 2.3.

In the first part of this paper, we aim at incorporating time delays in accumulation-based models to improve the representation of wave propagation and travel time evolution within the region. Then, new perimeter control algorithms should be designed to tackle not only uncertainties in MFD shapes, but also to compensate the delays. It should be stressed that in recent appeared papers (Haddad and Mirkin, 2016b; Keyvan-Ekbatani et al., 2012; Aboudolas and Geroliminis, 2013), travel times to the borders were incorporated as a time delay in the *control input* of the MFD-based models for control law synthesis. Unlike (Haddad and Mirkin, 2016b; Keyvan-Ekbatani et al., 2015), in this paper the delay is incorporated in the MFD dynamics as a state-delay.

Moreover, towards future real practical implementation, we also focus on an application-oriented problem related to delayed state interconnections. Note that in all above literature, it is implicitly postulated that all needed information for computing are obtained in real time and processed instantly. Apparently, in a real situation, it is difficult to complete all

the process at a glance, especially for large region networks, and there is a time delay because of different capacity of information transmission and process in traffic control centers. Hence, the second part of the paper aims at addressing this issue, in particular, *delayed state interconnections* are introduced in the dynamic equations to model data processing and communication delays between surrounding interconnected regions. The existence of pure time lags in the whole procedure may cause undesirable system transient response, or even instability.

The layout of this paper is as follows: first, state time-delay interpretations are given in Section 2, then two enhanced MFD accumulation-based models are developed by incorporating into model structure the time-delay effects as an important factor. In the first model, in Section 3, the time-delay is incorporated in the *MFD output function*, while *interconnection* time delay is integrated in the second model in Section 5. Based on the developed models, two coordinated distributed adaptive control schemes, introduced in Mirkin and Gutman (2003, 2005), are implemented to the first model in Section 4 and to the second model in Section 6. The two control schemes have different adaptation algorithms, as they differ in the used feedback information, i.e. one is a *state feedback* and the other is an *output feedback*, while both have the same control objective which is output tracking. Following the structure presented in Haddad and Mirkin (2017), the regional control laws are developed depending on (i) real on-line local information of the region, i.e. regional accumulation and its perimeter control input only, and (ii) reference model information forwarded to all decentralized perimeter controllers by a high level coordinator controller.

2. State time-delay interpretations in MFD accumulation-based models

In the following, we give a general description of the delay phenomenon, and its physical interpretations in MFD accumulation-based models for single-region systems.

2.1. Time delays

Time delays exist in various dynamic systems. There are transport and communication delays in mechanical, chemical, biological, and transportation systems (Marshall, 1992; Gu et al., 2003; Fridman, 2014). E.g., delays are a natural part of systems controlled via communication network due to buffering and propagation delays (Hespanha et al., 2007; Fridman, 2014; Gudin and Mirkin, 2007). Delays can also arise as a part of the system dynamics, e.g. complex dynamics can be approximated by relatively simple dynamics and a delay part (Zwart and Bontsema, 1997).

The continuous-time delay element D_τ can be defined as $y(t) = D_\tau x(t)$, which is equivalent to $y(t) = x(t-\tau)$, where the output signal $y(t)$ is the delayed, by τ (s), copy of the input signal $x(t)$.[1]

The MFD system is a classical application example in which time delays arise. Recently, in Haddad and Mirkin (2016b); Keyvan-Ekbatani et al. (2012); Aboudolas and Geroliminis (2013), travel times to the borders were incorporated as a time delay in the *control input* of the accumulation-based models for control law synthesis. In Keyvan-Ekbatani et al. (2012), for the gating control problem at *an urban region*, the time delay corresponds to the travel time needed for gated vehicles to approach the network is presented, while in Aboudolas and Geroliminis (2013) the control input delays are presented in the traffic flow dynamics for the perimeter control problem at *multi-region systems*. Note that the controller in Aboudolas and Geroliminis (2013) is designed assuming time delays equal to zero. In both cases the parameters of the system model are known, while the perimeter control in Haddad and Mirkin (2016b) is designed under unknown bounded external disturbances and parameter uncertainties. In the latter, the model reference adaptive control (MRAC) approach has been utilized to design the controllers. In both works, (Haddad and Mirkin, 2016b; Keyvan-Ekbatani et al., 2015), the perimeter controllers have been designed for *one region* MFD network.

In this paper, time delays are incorporated into the dynamics to enhance the accumulation-based models. Unlike previous works (Haddad and Mirkin, 2016b; Keyvan-Ekbatani et al., 2015), in the current paper the time delays are incorporated into the dynamic state, instead of the control input. Two types of delay are distinguished: (i) time delay in the regional MFD output, described in Section 2.2, and (ii) time delay in interconnections, described in Section 2.3.

2.2. Delayed MFD output in single-region systems

The accumulation-based dynamics for single-region systems has been first presented in Daganzo (2007). It has been the base for multi-region system dynamics with perimeter control in many works, e.g. in Geroliminis et al. (2013); Haddad and Mirkin (2016b, 2017); Aboudolas and Geroliminis (2013). We thus start with a brief description of the accumulation-based models for single-region systems, following the recent summarized description given in Mariotte et al. (2017).

The traffic flow state of an urban region network can be aggregately described by its accumulation $n(t)$ (veh), i.e. the number of circulating vehicles at time t. The traffic flow dynamics within the region is given by a relationship between the travel production $P(n(t))$ (veh · m/s) and the accumulation $n(t)$. The mean speed $V(n(t))$ of travelers (m/s) is given by $V(n(t)) = P(n(t))/n(t)$ at every time t, and the region outflow $G(n(t))$ (veh/s), i.e. trips ending in the region and trips exiting the region, satisfies the equation $G(n(t)) = P(n(t))/L$, where L (m) is the average vehicle trip length. Now, it is assumed that:

[1] In this paper only constant delays are considered.

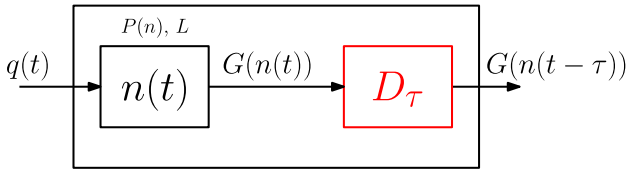

Fig. 1. Schematic representation of the single-region dynamics with delayed MFD output.

(A1) the total demand $q(t)$ (veh/s) for internal and transferring trips is less than the region capacity, (A2) the region outflow is not restricted by the supply at the network exits, (A3) the average vehicle trip length is the same for all origins, implying a proportional relationship between outflow and production, and (A4) the system demand evolves slowly over time. Then, under these assumptions, the evolution of the accumulation $n(t)$ is given by, according to Eq. (2) in Daganzo (2007),

$$\dot{n}(t) = q(t) - G(n(t)) . \tag{1}$$

Note that (A2) should be mainly considered in multi-region systems, and it can be relaxed e.g. by imposing boundary capacity constraints (Ramezani et al., 2015). Several research works have analyzed (A3), as the effect of trip lengths on the accumulation-based model was investigated in Yildirimoglu and Geroliminis (2014); Leclercq et al. (2015); Mariotte et al. (2017); Geroliminis (2015). In Leclercq et al. (2015), it was observed that assuming vehicle trip lengths constant for all vehicles is not consistent, when the local dynamics are taken into account, since trip lengths depend also on the traffic condition within the region. On the other hand, (Geroliminis, 2015) proposed to include different trip length classes in the accumulation-based framework to tackle this issue. Unlike the accumulation-based models as vehicles entering the region will keep the same average speed until they exit, the key idea in trip-based models (Arnott, 2013; Fosgerau, 2015; Lamotte and Geroliminis, 2016; Mariotte et al., 2017) is to guaranty that all vehicles cover their travel distance within the region by adjusting the instantaneous speed to the current regional mean speed defined by the MFD (Mariotte et al., 2017). Finally, according to Daganzo (2007), the region outflow, represented by the MFD function, describes steady-state (equilibrium) behavior but can be used for dynamic analysis, if the inputs change slowly, i.e. (A4). The recent work (Mariotte et al., 2017) describes the validity domain of the accumulation-based models in terms of demand gap and gap duration.

The transitions between steady states due to input changes are not instantaneous, e.g. as stated in the footnote 2 in Daganzo (2007) "If flow is increased on an empty link, its outflow and accumulation do not reach a steady state immediately, there is a delay". In other words, vehicles reaching the destination at the current time t, i.e. $G(n(t))$, are those vehicles that already started their trip earlier than time t and only now at time t they are reaching the destination, since clearly vehicles can not *immediately* travel from the urban region to its border with infinite speeds. Hence, an enhanced model would be to incorporate a time delay in the region output within the accumulation-based modeling approach. In this way, if the flow varies rapidly, e.g. in terms of demand gap and gap duration, refer to Mariotte et al. (2017), the MFD outflow will be delayed, and hence it will not react too fast. The MFD accumulation-based dynamics for single-region systems with delayed MFD output can be described as follows, see also Fig. 1,

$$\dot{n}(t) = q(t) - G(n(t - \tau(t))), \tag{2}$$

where, $\tau(t)$ is the average travel time for all vehicles, which can be calculated according to the regional MFD as follows

$$\tau(t) = \frac{L(t)}{V(n(t))} = \frac{n(t)}{G(n(t))}. \tag{3}$$

Note that the delay is a state-dependent, i.e. $\tau(n(t))$. Increasing the steady state demand from q_{eq} to $q_{\text{eq}} + \Delta q$ would move the current steady state (an equilibrium point) n_{eq}, i.e. the corresponding accumulation state for which it holds that $\dot{n}(t) = 0$, to $n_{\text{eq}} + \Delta n$, and τ would also change over the state $n(t)$. In this paper, we focus on designing perimeter control for accumulation-based models with constant delays. It should be stressed that time varying delays can be also considered in the same control design framework, since the function of time delay is known in advance. Treating time varying state delays would be a future research topic.

Based on the MFD, the average time delay $\overline{\tau}$ (s) can be calculated as

$$\overline{\tau} = \frac{\int_{n_{\text{eq}}}^{n_{\text{eq}}+\Delta n} \tau(n)\mathrm{d}n}{\Delta n}. \tag{4}$$

Note that the average time delay depends on the current steady state n_{eq} and the increase in state value, Δn. Assuming a third polynomial shape of the MFD, i.e. $G(n) = a \cdot n^3 + b \cdot n^2 + c \cdot n$, refer to Geroliminis and Daganzo (2008), then the $\tau(n(t))$ function and the average time delay $\overline{\tau}$ are depicted schematically in Fig. 2, where n_{jam} denotes the jammed accumulation.

It should be stressed that other realizations of average time delay can be also considered. E.g., since we mainly operate around equilibrium points, one can also consider the regional time delay as a constant average value obtained at the equilibrium point, i.e. $\tau = \tau(n_{\text{eq}})$. The aim of the current work is to design perimeter control that can compensate average time delays in the dynamics states.

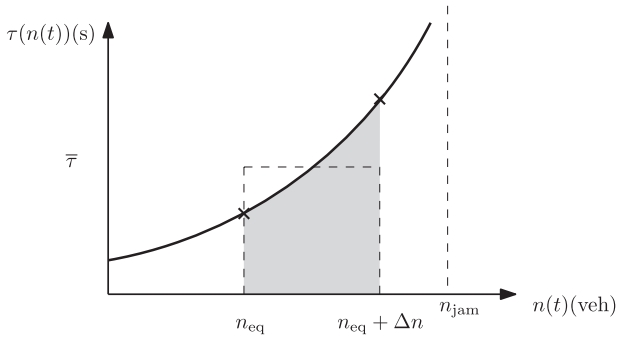

Fig. 2. Travel time (time delay) as a function of $n(t)$ within the range $[0, n_{\text{jam}}]$.

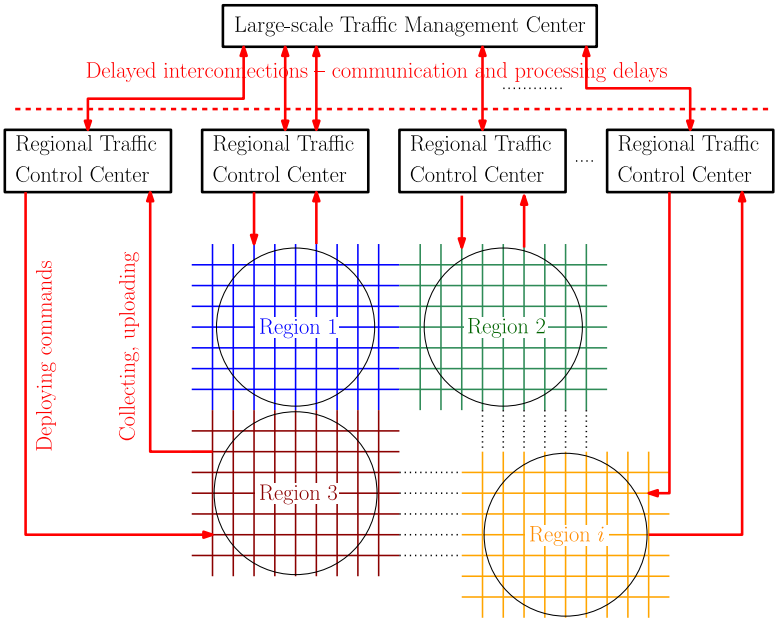

Fig. 3. Distributed adaptive perimeter control scheme with delayed interconnections: A large-scale traffic management center that coordinates between traffic control centers for urban regions (based on Haddad and Mirkin, 2017).

2.3. Delayed interconnections

In general, traffic control management includes three tasks: (i) collecting traffic data from various sensors, (ii) processing the collected data, and (iii) deploying mechanisms for controlling network traffic. Collecting, processing, and uploading traffic data in large-scale urban road networks impose time delays.

Usually, a large-scale urban road network has a main traffic management center, see Fig. 3, which has several distributed regional traffic control centers. Each regional traffic control center has various sensors and detectors that collect traffic data. The collected data are first uploaded to the regional center, then they are processed by different estimation methods and algorithms to estimate the state of the system, e.g. to estimate the accumulation in the region, or to evaluate performance indices. Collecting, uploading, and processing the data within the region impose time delays in the dynamics of that region. The value of this time delay depends on several factors, mainly the regional traffic characteristics, e.g. network size and structure, and the monitoring system properties of the control center, e.g. type of sensors. Once the data is processed, each regional center will transfer the data and information to the main traffic management center, probably implying another communication delays. Receiving data and information from all sub-networks, that have different communication properties, will also impose communication delays. Finally, the main traffic management center will send commands and instructions to the regional control centers to coordinate the vehicle numbers in the regions. Again, the latter might impose computational and communication delays. In this paper, we focus our investigation on the computational and communication delays which are imposed while transferring the data and information from one region to another region through the management center. Hence, these time delays are incorporated in the accumulation-based dynamics as *delayed state interconnections*, to model data processing and communication delays between surrounding interconnected regions.

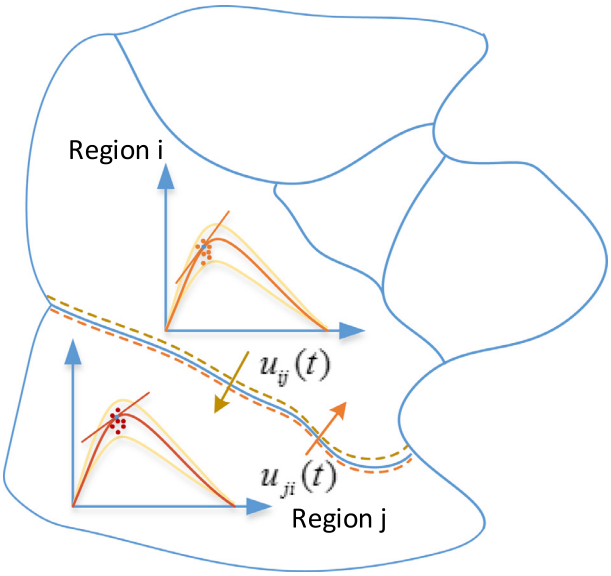

Fig. 4. An urban network with multiple regions, each having uncertain MFD.

For a better understanding, we give our observations from two traffic management centers in Jerusalem and Tel Aviv. Our observations in Jerusalem traffic management center show that several seconds of delay are observed while executing communicational or computational application. In other words, e.g. sending data to Tel Aviv traffic management center it will be received after a time lag. Note that another possible reason for communication time delay would be encrypting the data before sending it to another traffic center. These type of actions impose time delays in the interconnections between the regions. Note that in Jerusalem traffic management center, collected data from sensors are sent every second to the center, and these data are aggregated based on a minute mark if the link is not associated with a signalized intersection, or based on the cycle time if the link is associated with a signalized intersection. Because of data backup space limitation, only aggregated data over 15 min are saved in the control system. Such aggregated data can be utilized in the system to run several applications. On the other hand, the system in Tel Aviv traffic management center is operated differently, where data is locally collected at the level of the induction-loop detectors of the signalized intersections. The Tel Aviv traffic center does not receive raw data every second, but it only gets aggregated data every 5min from the loop detectors. Here, one can realize that the aggregation time for collected data might be different for traffic centers, e.g. 5 min in Tel Aviv versus 15 min in Jerusalem. The difference between these aggregation times would be crucial in MFD application, given the fact that the MFD dynamics are based on aggregated data of accumulation. This is another interesting problem that should be addressed in a future research. Nevertheless, the presented framework might be also utilized to tackle this issue, as the difference between aggregation times might be modeled as data fusing with time delays in the system.

3. Accumulation-based models with delayed MFD output

An enhanced accumulation-based dynamic model with delayed MFD outputs for R interconnected regions is presented. The presented model is based on the model developed in Geroliminis et al. (2013); Haddad and Mirkin (2017).

3.1. Basic nonlinear accumulation-based model for multiple regions

Let us consider a large-scale urban network decomposed into R homogeneous urban subnetworks (regions), each having uncertain MFD, as shown in Fig. 4. Let us denote $q_{ij}(t)$ (veh/s) as the traffic flow demand generated in region i with direct destination to region j. Here $i = 1, \ldots, R$ and $j \in S_i$, where S_i defines the set of regions, with which the region i can communicate, i.e. the set of regions that are directly reachable from region i. Each of S_i is a set of integers corresponding to the region's index number. Corresponding to the traffic demands, the dynamical system states (accumulations) are defined as: $n_{ii}(t)$ (veh) is the total number of vehicles in region i with destination to inside the region; $n_{ij}(t)$ (veh) is the total number of vehicles in region i with direct destination to region j; and $n_i(t)$ (veh) is the accumulation or the total number of vehicles in region i, that is

$$n_i(t) = n_{ii}(t) + \sum_{j \in S_i} n_{ij}(t)\,. \tag{5}$$

The vehicle conservation equations of the R-region system are as follows, based on Geroliminis et al. (2013); Haddad and Mirkin (2016b, 2017),

$$\dot{n}_{ii}(t) = -M_{ii}(n_{ii}(t), n_i(t)) + \sum_{j\in S_i} M_{ji}(n_{ji}(t), n_j(t))u_{ji}(t) + q_{ii}(t)\,,$$
$$\dot{n}_{ij}(t) = -M_{ij}(n_{ij}(t), n_i(t))u_{ij}(t) + q_{ij}(t),\ j \in S_i \tag{6}$$

where the variables $M_{ij}(n_{ij}(t),\ n_i(t))$ (veh/s) and $M_{ji}(n_{ji}(t),\ n_j(t))$ (veh/s) denote the transfer flows with the corresponding direction, i.e. from region i to j and from region j to i, respectively. Based on the MFD concept, the internal, input and output traffic flows of region i can be calculated corresponding to some relationships between accumulations, see (Haddad and Mirkin, 2016b; Geroliminis et al., 2013), namely in the form of the following weighted nonlinear relations,

$$M_{ii}(n_{ii}(t), n_i(t)) = \frac{n_{ii}(t)}{n_i(t)} G_i(n_i(t)) - [\text{flow with internal direction}], \tag{7}$$

$$M_{ij}(n_{ij}(t), n_i(t)) = \frac{n_{ij}(t)}{n_i(t)} G_i(n_i(t)) - [\text{transfer flow with direction from } i \text{ to } j,\ j \in S_i], \tag{8}$$

$$M_{ji}(n_{ji}(t), n_j(t)) = \frac{n_{ji}(t)}{n_j(t)} G_j(n_j(t)) - [\text{transfer flow with direction from } j \text{ to } i,\ i \in S_j], \tag{9}$$

where $G_i(n_i(t))$ (veh/s) denotes the appropriate MFD parametrization for region i, i.e. the nonlinear relationship between the trip completion flow G_i and the accumulation $n_i(t)$ (veh).

To be able to regulate the transfer flows $M_{ij}(n_{ij}(t),\ n_i(t))$ and $M_{ji}(n_{ji}(t),\ n_j(t))$ at the perimeter border of region i, we define the transfer flows as adjustable controlled flows in the following form:

$$M_{ij}(n_{ij}(t), n_i(t))u_{ij}(t) - [\text{controlled flow from } i \text{ to } j,\ j \in S_i], \tag{10}$$

$$M_{ji}(n_{ji}(t), n_j(t))u_{ji}(t) - [\text{controlled flow from } j \text{ to } i,\ i \in S_j], \tag{11}$$

where the variables $u_{ji}(t)$ and $u_{ij}(t)$ represent the perimeter control inputs, which are introduced on the border between the regions i and j as shown in Fig. 4, to control the transfer flows between the regions.

3.2. Nonlinear accumulation-based multi-region model with delayed MFD outputs

Note that in (6), as in most of the known accumulation-based MFD dynamic models that are utilized for *control design*, it is implicitly postulated that vehicles reaching the destination at the current time t, i.e. $G_i(n_i(t))$, are those vehicles that already started their trip earlier than time t and only now at time t they are reaching the destination, since clearly vehicles can not *immediately* travel from the urban region to its border with infinite speeds. The travel time needed for vehicles to reach their destinations should be inherently integrated in the dynamic equations of the system.

Following the aggregated dynamic modeling approach, one can postulate that the average travel time for all vehicles traveling towards destination can be calculated according to the regional MFD, see (3). Considering a constant average travel time for region i, i.e. τ_i (s), which can be calculated from (4), the constant time delays are then incorporated to the MFD output functions as follows

$$G_i(n_i(t-\tau_i)) = a_i \cdot n_i^3(t-\tau_i) + b_i \cdot n_i^2(t-\tau_i) + c_i \cdot n_i(t-\tau_i)\,. \tag{12}$$

Given (12), we re-write the dynamic model of the multi-region system (6) with *delayed MFD outputs*, as follows

$$\dot{n}_{ii}(t) = q_{ii}(t) + \sum_{j\in S_i} \frac{n_{ji}(t)}{n_j(t)} \cdot G_j(n_j(t-\tau_j)) \cdot u_{ji}(t) - \frac{n_{ii}(t)}{n_i(t)} \cdot G_i(n_i(t-\tau_i))\,, \tag{13}$$

$$\dot{n}_{ij}(t) = q_{ij}(t) - \sum_{j\in S_i} \frac{n_{ij}(t)}{n_i(t)} \cdot G_i(n_i(t-\tau_i)) \cdot u_{ij}(t), \tag{14}$$

$$n_i(t-\tau_i) = n_{ii}(t-\tau_i) + \sum_{j\in S_i} n_{ij}(t-\tau_i)\,, \tag{15}$$

and (5),

where $i, j = 1, 2, \ldots R,\quad j \in S_i$.

3.3. Linearized model for adaptive perimeter control design

To deal with the traffic dynamics of the nonlinear model, i.e (13)–(15) and (5), we linearize the model at an equilibrium point $(n_{ij,\,eq}, q_{ij,\,eq}, u_{ij,\,eq})$, $i, j = 1, 2, \cdots, R$, and follow the coupled control scheme in Haddad and Mirkin (2016b), i.e. $u_{ij}(t) + u_{ji}(t) = \epsilon$, guarantying that boundary capacity is split between the two directions. Then, the linearized state space model, which are composed of interconnected regions with set of unknown parameters, can be written as

$$\begin{aligned} \dot{x}_i(t) &= A_i x_i(t) + \tilde{A}_i x_i(t-\tau_i) + B_i u_i(t) + \sum_{j\in S_i} A_{ij} x_j(t) + \sum_{j\in S_i} \tilde{A}_{ij} x_j(t-\tau_j), \\ y_i(t) &= n_i(t) = c_i^T x_i(t), \quad c_i^T = \underbrace{[1, \cdots, 1]}_{\text{card}(S_i)+1}, \; i = 1, \cdots, R, \end{aligned} \tag{16}$$

where $x_i(t) = [\Delta n_{ii}(t), \ldots, \Delta n_{ij}(t), \ldots]^{\mathrm{T}} \in \mathrm{R}^{(\dim(S_i)+1)\times 1}$ with $\Delta n_{ij}(t) = n_{ij}(t) - n_{ij,\mathrm{eq}}$, $j \in S_i$; $u_i(t) = [\Delta u_{ii}(t), \ldots, \Delta u_{ij}(t), \ldots]^{\mathrm{T}} \in \mathrm{R}^{(\dim(S_i)+1)\times 1}$ with $\Delta u_{ij}(t) = u_{ij}(t) - u_{ij,\mathrm{eq}}$, $j \in S_i$; $\tilde{x}_j(t-\tau_j) = [\Delta n_{jj}(t-\tau_j), \ldots, \Delta n_{ji}(t-\tau_j), \ldots]^{\mathrm{T}} \in \mathrm{R}^{(\dim(S_j)+1)\times 1}$ with $\Delta n_{ji}(t-\tau_j) = n_{ji}(t-\tau_j) - n_{ji,\mathrm{eq}}$, $i, j = 1, 2, \cdots, R$, $i \neq j$, which are the interconnected elements with delay. The constant system parameter matrices $A_i \in \mathbb{R}^{(1+card(S_i))\times(card(S_i)+1)}$, $B_i \in \mathbb{R}^{(1+card(S_i))\times card(S_i)}$, $A_{ij} \in \mathbb{R}^{(1+card(S_i))\times(card(S_j)+1)}$, $\tilde{A}_i$, $\tilde{A}_{ij}$ are being *unknown*, and τ_i, $i = 1, \cdots, R$, are known time delays. Note that $\Delta u_{ii}(t)$ are auxiliary variables, which are added to adapt our problem to the general form in (16), where $\Delta u_{ii}(t) = \sum_j b_j \Delta u_{ji}(t)$, $j \in S_i$, with coefficients b_j which are calculated after linearization.

The system dynamics given by (16) is used for distributed adaptive control design. For control synthesis it is assumed that the parameters matrices of (16) are *unknown* due to varying external conditions (plant with parametric uncertainties). Therefore, in order to accommodate the parametric uncertainties and compensate for the delayed MFD output, adaptive control is designed.

4. Adaptive perimeter control I: control design for accumulation-based models with delayed MFD outputs

In the following, the perimeter control is designed according to the proposed control design in Mirkin and Gutman (2003). The control scheme is state feedback for output tracking. Typical assumptions on the plant as it is usual in model reference adaptive control (MRAC) are also assumed here. For a detailed information, the reader can refer to Mirkin and Gutman (2003).

4.1. Control objective and reference models

Our control objective is to construct distributed local state feedback control laws $u_i(t)$ in (16) to make all the closed-loop signals bounded, and the output signals $y_i(t)$ asymptotically track given reference signals $y_{mi}(t) \in \mathbb{R}$ from stable local reference models

$$\begin{aligned} \dot{x}_{mi}(t) &= A_{mi} x_{mi}(t) + B_{mi} r_i(t), \\ y_{mi}(t) &= c_i^T x_{mi}(t), \quad c_i^T = [1, \ldots, 1], \; i = 1, \ldots, R, \end{aligned} \tag{17}$$

where for the ith model, $x_{mi}(t)$ is the state vector, and $r_i(t) \in \mathbb{R}$ is an appropriate reference input allowing the region output $y_i(t)$ to be equal to the desired signal $y_{mi}(t)$. The matrices A_{mi} and B_{mi} are known constant matrices of appropriate dimensions.

The desired pair of matrices A_{mi}, B_{mi} in (17) are selected such that the reference model has a fast dynamics, and so it shortly provides a desired constant output n_i^*. Usually, the objective of control is to make $n_i(t)$ tends to $n_{mi}(t)(= n_i^*)$ asymptotically, i.e. $n_i(t) \to n_i^*$ if $t \to \infty$ for $i = 1, \ldots, R$. However, other objectives can be defined e.g. tracking accumulation trajectories which vary with time, see e.g. numerical Example 4 in Section 7.

4.2. Distributed adaptive controller structure

The distributed adaptive control scheme with *reference model coordination*, refer to e.g. (Mirkin, 2003; Mirkin and Gutman, 2003; Mirkin et al., 2012), is used to achieve the control objective. The control law for the ith region $u_i(t)$ is chosen to be of the form

$$u_i(t) = u_{li}(t) + u_{ci}(t), \quad i = 1, \cdots, R, \tag{18}$$

where the component $u_{li}(t)$ is based only on *local* signals of the ith region, and $u_{ci}(t)$ is the *coordinated* feedforward component which is based on the reference signals of all the other regions. To anticipate the uncertainty effects, suitable parameterizations of the local and coordinated components of the control law (18) should be defined. In this paper, we follow the parameterizations defined in Mirkin and Gutman (2003), which are described here as follows.

4.2.1. Control component based only on local information:

The part of the control law, $u_{li}(t)$, which is based only on the local information is parameterized as follows,

$$\begin{aligned} u_{li}(t) &= K_i^T(t)\omega_{li}(t)\,, \\ w_{li}(t) &= \left[e_i(t), x_{pi}^T(t), x_{li}^T(t), r_i(t)\right]^T, \\ \dot{x}_{li}(t) &= F_i x_{li}(t) + g_i y_i(t)\,, \qquad \dot{x}_{pi}(t) = F_i x_{pi}(t) + g_i u_i(t)\,, \end{aligned} \tag{19}$$

where $e_i(t) = y_i(t) - y_{mi}(t)$, (F_i, g_i) is a minimal state space representation of the transfer function of the reference model, and x_{pi} includes all the plant states of region i, while x_{li} includes only the local states of region i. The controller in (19) uses only the measured local system outputs $y_i(t)$.

4.2.2. Coordinated feedforward control component:

The coordinated control feedforward component $u_{ci}(t)$ is defined as a linear combination of *the states of the reference models* with the following dynamic adaptive pre-filter:

$$\begin{aligned} u_{ci}(t) &= -\sum_{j\in S_i}\left[K_{mij}^T(t)\omega_{mij}(t) - K_{zij}^T(t)\omega_{zij}(t)\right], \\ \omega_{mij}(t) &= \left[x_{mj}^T(t)\;\; x_{mj}^T(t-\tau_j)\right]^T, \qquad \omega_{zij}(t) = \left[z_{mij}^T(t)\;\; z_{m\tau ij}^T(t)\right]^T, \\ \dot{z}_{mij}(t) &= F_{di} z_{mij}(t) + g_{di} x_{mj}(t)\,, \quad \dot{z}_{m\tau ij}(t) = F_{di} z_{m\tau ij}(t) + g_{di} x_{mj}(t-\tau_j)\,, \end{aligned} \tag{20}$$

where $K_{mij}(t)$, $K_{zij}(t)$ are time-varying adaptation gain vectors, and $F_{di} = \mathrm{diag}\{F_i\}$ and $g_{di} = \mathrm{diag}\{g_i\}$.

4.2.3. Adaptation algorithms:

The adaptation algorithms are chosen as follows,

$$\dot{K}_i(t) = -\mathrm{sign}\left(\frac{k_{pi}}{k_{mi}}\right)\Gamma_{ii} e_i(t)\omega_{li}(t)\,, \tag{21}$$

$$\dot{K}_{mij}(t) = \mathrm{sign}\left(\frac{k_{pi}}{k_{mi}}\right)\Gamma_{mi} e_i(t)\omega_{mij}(t)\,, \tag{22}$$

$$\dot{K}_{zij}(t) = -\mathrm{sign}\left(\frac{k_{pi}}{k_{mi}}\right)\Gamma_{zi} e_i(t)\omega_{zij}(t)\,, \tag{23}$$

where Γ_{ii}, Γ_{mi}, Γ_{zi} are from the Lyapunov function Eq. (18) in Mirkin and Gutman (2003) which should be tuned, k_{pi} and k_{mi} are respectively known constant gains in the transfer functions for the plant $W_i(s)$ and the reference model $W_{mi}(s)$, i.e.

$$W_i(s) = k_{pi}\frac{N_i(s)}{D_i(s)}\,, \qquad W_{mi}(s) = k_{mi}\frac{N_{mi}(s)}{D_{mi}(s)}\,, \tag{24}$$

where $N_i(s)$, $D_i(s)$, $N_{mi}(s)$, $D_{mi}(s)$ are monic polynomials.

Consider the system in (16) and the reference models in (17). Then, according to Theorem 1 in Mirkin and Gutman (2003), the distributed adaptive perimeter control (18)–(20) with adaptation rules (21)–(23) assure that (i) the closed-loop signals are bounded, and (ii) all tracking errors $e_i(t), i = 1, \ldots, R$, converge to zero asymptotically. Therefore, the local outputs $y_i(t)$ asymptotically track the reference model outputs $y_{mi}(t)$. The reference model dynamics can be chosen such that the local outputs $y_i(t)$ track specified external signals e.g. constants.

5. Accumulation-based models with delayed interconnections

In this section, an enhanced accumulation-based dynamic model with delayed interconnections is developed.

5.1. Nonlinear MFD model with delayed interconnected subsystems

For simplicity, the delayed interconnections between regions are assumed to be constant values. Hence, considering region i, a time delay τ_j is added to the *interconnection elements* in the dynamic equations from region j to region i: (i) the MFD output function of region j, $j \in S_i$, i.e. $G_j(n_j(t-\tau_j))$, and (ii) the accumulations at region j, i.e. $n_{jj}(t-\tau_j)$, $n_{ji}(t-\tau_j)$, $n_j(t-\tau_j)$. Then, we can re-write the dynamic model (6) with *delays in interconnections* as follows

$$\dot{n}_{ii}(t) = q_{ii}(t) + \sum_{j\in S_i}\frac{n_{ji}(t-\tau_j)}{n_j(t-\tau_j)}\cdot G_j(n_j(t-\tau_j))\cdot u_{ji}(t) - \frac{n_{ii}(t)}{n_i(t)}\cdot G_i(n_i(t))\,, \tag{25}$$

$$\dot{n}_{ij}(t) = q_{ij}(t) - \sum_{j\in S_i}\frac{n_{ij}(t)}{n_i(t)}\cdot G_i(n_i(t))\cdot u_{ij}(t)\,, \tag{26}$$

$$n_i(t) = n_{ii}(t) + \sum_{j\in S_i} n_{ij}(t)\,, \tag{27}$$

$$n_j(t-\tau_j) = n_{jj}(t-\tau_j) + \sum_{i\in S_j} n_{ji}(t-\tau_j)\,, \tag{28}$$

where $i = 1, 2, \ldots R$, $j \in S_i$.

5.2. Linearized model for adaptive control design

In order to deal with the nonlinear model with delayed interconnected subsystems described in (25)–(28), we linearize the nonlinear model at an equilibrium point $(n_{ij,\,\mathrm{eq}},\ q_{ij,\,\mathrm{eq}},\ u_{ij,\,\mathrm{eq}})$, $i, j = 1, 2, \ldots, R$. Then, the linearized state space model, which is composed of interconnected regions can be written as

$$\dot{x}_i(t) = A_i x_i(t) + B_i u_i(t) + \sum_{j\in S_i} \tilde{A}_{ji}\tilde{x}_j(t-\tau_j)\,, \tag{29}$$

where $x_i(t) = [\Delta n_{ii}(t), \ldots, \Delta n_{ij}(t), \ldots]^{\mathrm{T}} \in \mathrm{R}^{(\dim(S_i)+1)\times 1}$ with $\Delta n_{ij}(t) = n_{ij}(t) - n_{ij,\mathrm{eq}}$, $j \in S_i$; $u_i(t) = [\Delta u_{ii}(t), \ldots, \Delta u_{ij}(t), \ldots,]^{\mathrm{T}} \in \mathrm{R}^{(\dim(S_i+1))\times 1}$ with $\Delta u_{ij}(t) = u_{ij}(t) - u_{ij,\mathrm{eq}}$, $j \in S_i$; $\tilde{x}_j(t-\tau_j) = [\Delta n_{jj}(t-\tau_j), \ldots, \Delta n_{ji}(t-\tau_j), \ldots]^{\mathrm{T}} \in \mathrm{R}^{(\dim(S_j)+1)\times 1}$ with $\Delta n_{ji}(t-\tau_j) = n_{ji}(t-\tau_j) - n_{ji,\mathrm{eq}}$, $i, j = 1, 2, \ldots, R$, $i \neq j$, which are the interconnected elements with delay. Matrices A_i, B_i, and $\tilde{A}_{ji}$ are matrices of proper dimensions. Here, we also add $\Delta u_{ii}(t)$ as auxiliary variables to adapt our problem to the form in (29), where $\Delta u_{ii}(t) = \sum_j b_j \Delta u_{ji}(t)\,,\ j \in S_i$, with coefficients b_j which are calculated after linearization. It should be noted that one can derive the form in (29) from the general form presented in (16) by choosing appropriate matrices.

6. Adaptive perimeter controller II: control design for accumulation-based models with delayed interconnections

The control objective, the reference models, and the controller structure are the same as those proposed in Section 4. Note, however, that the plant models have different forms, i.e. the linearized model (29) has a different form compared with the linearized model introduced in (16), and the control scheme which has been followed here is output feedback for output tracking. Hence, different adaptation control rules are introduced compared with Section 4.

6.1. Control objective, reference models, and control structures

The control objective is to design distributed local state feedback control laws $u_i(t)$ in (29) to make all the closed-loop signals bounded, and the output signals $y_i(t) = x_i(t)$ asymptotically track given reference signals $y_{ri}(t) = x_{ri}(t)$ with stable local reference model input $r_i(t)$. The reference model for region i is given by $\dot{x}_{ri}(t) = A_{ri}x_{ri}(t) + B_{ri}r_i(t)$, where $x_{ri}(t) \in \mathrm{R}^{(\dim(S_i)+1)\times 1}$ is the state vector, and $r_i(t) \in \mathrm{R}^{(\dim(S_i)+1)\times 1}$ is an appropriate reference input. Matrices A_{ri} and B_{ri} are known constant matrices of proper dimensions.

The distributed adaptive control scheme with reference model coordination is used to achieve the control objective. The control law for the ith local subsystem $u_i(t)$ is chosen to be of the form (18). The parameterizations of local and coordinated components of the control law in (18) are defined according to the ones proposed in Mirkin and Gutman (2005), which are briefly summarized as follows. Typical assumptions on the plant as it is usual in model reference adaptive control (MRAC), see (Mirkin and Gutman, 2005), are also assumed here.

6.2. Control law parametrizations

6.2.1. Control component on local information

The part of the control law, which is based only on local information is parameterized as follow

$$u_{li}(t) = \theta_{li}^{*\mathrm{T}}\omega_{li}(t) = \theta_{fi}^{*\mathrm{T}}\omega_{fi}(t) + \theta_i^{*\mathrm{T}}\omega_i(t), \tag{30}$$

where $\theta_{li}^{*\mathrm{T}} = [\theta_{fi}^{*\mathrm{T}} \quad \theta_i^{*\mathrm{T}}]$, $\theta_{fi}^{*\mathrm{T}} = [\theta_{ei}^{*} \quad \theta_{1i}^{*\mathrm{T}} \quad \theta_{2i}^{*\mathrm{T}}]$, $\theta_i^{*\mathrm{T}} = [\theta_{r1i}^{*} \quad \theta_{r2i}^{*}]$, θ_{ei}^{*}, $\theta_{1i}^{*\mathrm{T}}$, $\theta_{2i}^{*\mathrm{T}}$, θ_{r1i}^{*}, θ_{r2i}^{*} are some constant parameter matrices. $\omega_{fi}(t)$ and $\omega_i(t)$ are the local feedback and local feedforward signals, respectively, which are given by

$$\omega_{fi}(t) = \begin{bmatrix} I_{mi} & 0 & 0 \\ 0 & \Phi_i(s) & 0 \\ 0 & 0 & \Phi_i(s) \end{bmatrix} \begin{bmatrix} e_i(t) \\ y_i(t) \\ u_i(t) \end{bmatrix}, \tag{31}$$

$$\omega_i(t) = \begin{bmatrix} I_{mi} \\ W_{ri}(s) \end{bmatrix} r_i(t), \tag{32}$$

where $\Phi_i(s) = \frac{[I_{mi}s^{\nu_i-1},\ldots,I_{mi}s,I_{mi}]^{\mathrm{T}}}{\Lambda_i(s)}$, I_{mi} is an identity matrix, $i, j = 1, 2, \ldots, R$, $\Lambda_i(s) = s^{\nu_i-1} + \cdots + \lambda_{mi}s + \lambda_{0i}$ is a monic Hurwitz polynomial, ν_i denotes the observability index of $W_i(s)$, and $W_{ri}(s)$ and $W_i(s)$ are respectively the transfer functions of the reference model and the plant for region i.

6.2.2. Coordinated feedforward control component

The coordinated control component is based on the reference signals of all other subsystems, as follows

$$u_{ci}(t) = \sum_{j\in S_i} \theta_{ij}^{*\mathrm{T}}\omega_{ij}(t), \tag{33}$$

$$\dot{Z}_{rij}(t) = A_{\phi ij}Z_{rij}(t) + B_{\phi ij}y_{rj}(t-\tau_j)\,, \tag{34}$$

$$z_{rij}(t) = C_{\phi ij}Z_{rij}(t)\,, \tag{35}$$

$$\omega_{ij}(t) = \left[z_{rij}^{\mathrm{T}}(t) \quad y_{rj}^{\mathrm{T}}(t-\tau_j)\right]^{\mathrm{T}}, \tag{36}$$

where $(A_{\phi ij}, B_{\phi ij}, C_{\phi ij})$ is a minimal state space realization for a stable transfer matrix, $\theta_{ij}^{*\mathrm{T}} = [\theta_{1ij}^{*\mathrm{T}} \quad \theta_{2ij}^{*\mathrm{T}}]$, $\theta_{1ij}^{*\mathrm{T}}$, $\theta_{2ij}^{*\mathrm{T}}$ are some constant parameter matrices.

6.3. Adaptation algorithms

To develop an adaptation law for the controller in (18), the closed-loop system in terms of the tracking error $e_i(t) = y_i(t) - y_{ri}(t)$ is derived as in Mirkin and Gutman (2005)

$$e_i(t) = W_{ri}(s)K_{pi}\left[u_i(t) - \theta_{li}^{*\mathrm{T}}\omega_{li}(t) - \sum_{j\in S_i}\theta_{ij}^{*\mathrm{T}}\omega_{ij}(t) + \sum_{j\in S_i}(A_{ij}^{*}e_j(t-\tau_j) - A_{zij}^{*}\Phi_{ij}(s)e_j(t-\tau_j))\right], \tag{37}$$

where $\omega_{li}(t) = [\omega_{fi}(t)\,\omega_i(t)]^T$, K_{pi} is the high frequency gain matrix of region i, and $K_{pi} = \lim_{s\to\infty} sW_i(s)$. Finally, the adaptation algorithm is chosen as follows

$$\begin{aligned}
\dot{\theta}_{li}(t) &= -\eta_i(t) - \dot{\eta}_i(t) - \dot{\eta}_i(t-h_i)\,,\\
\eta_i^{\mathrm{T}}(t) &= \gamma_i S_{pi}e_i(t)\omega_{li}^{\mathrm{T}}(t)\,,\\
\dot{\theta}_{ij}(t) &= -\eta_{ij}(t)\,,\\
\eta_{ij}^{\mathrm{T}}(t) &= \gamma_{ij}S_{pi}e_i(t)\omega_{ij}^{\mathrm{T}}(t)\,.
\end{aligned} \tag{38}$$

The matrix S_{pi} is constant, chosen according to the condition of $K_{pi}S_{pi} = (K_{pi}S_{pi})^{\mathrm{T}} > 0$, h_i, γ_i, γ_{ij} are some constant traditional gains.

7. Numerical examples: adaptive perimeter control with delayed output for two urban regions

In this section, results of several numerical examples are presented to explore the features of the adaptive perimeter control I, i.e. (18)–(23), for an MFD system of two regions with delayed MFD outputs, see (A.1)–(A.8), under different traffic conditions.

7.1. Linearized two-region model for adaptive perimeter control design

Following (16), the linearized state space model for the two-region system can be written as

$$\begin{aligned}
\dot{x}_1(t) &= A_1x_1(t) + \tilde{A}_1x_1(t-\tau_1) + b_1u_1(t) + A_{12}x_2(t) + \tilde{A}_{12}x_2(t-\tau_2),\\
y_1(t) &= c_1^Tx_1(t),\ c_1 = [1,1]^T,\\
\dot{x}_2(t) &= A_2x_2(t) + \tilde{A}_2x_2(t-\tau_2) + b_2u_2(t) + A_{21}x_1(t) + \tilde{A}_{21}x_1(t-\tau_1)\,,\\
y_2(t) &= c_2^Tx_2(t),\ c_2 = [1,1]^T,
\end{aligned} \tag{39}$$

where

$$x_1(t) = \begin{bmatrix}\Delta n_{11}(t)\\ \Delta n_{12}(t)\end{bmatrix} = \begin{bmatrix}n_{11}(t) - n_{11,\mathrm{eq}}\\ n_{12}(t) - n_{12,\mathrm{eq}}\end{bmatrix} \in \mathbb{R}^2, \quad x_2(t) = \begin{bmatrix}\Delta n_{22}(t)\\ \Delta n_{21}(t)\end{bmatrix} = \begin{bmatrix}n_{22}(t) - n_{22,\mathrm{eq}}\\ n_{21}(t) - n_{21,\mathrm{eq}}\end{bmatrix} \in \mathbb{R}^2,$$

$$x_1(t-\tau_1) = \begin{bmatrix}\Delta n_{11}(t-\tau_1)\\ \Delta n_{12}(t-\tau_1)\end{bmatrix} = \begin{bmatrix}n_{11}(t-\tau_1) - n_{11,\mathrm{eq}}\\ n_{12}(t-\tau_1) - n_{12,\mathrm{eq}}\end{bmatrix} \in \mathbb{R}^2,$$

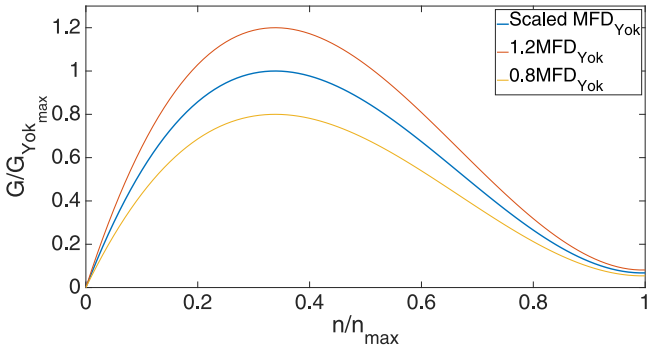

Fig. 5. Three shapes of MFD: (1) nominal scaled shape Yokohama MFD, i.e. MFD_{Yok}, (2) $1.2\text{MFD}_{\text{Yok}}$, (3) $0.8\text{MFD}_{\text{Yok}}$.

$$x_2(t-\tau_2)=\begin{bmatrix}\Delta n_{22}(t-\tau_2)\\ \Delta n_{21}(t-\tau_2)\end{bmatrix}=\begin{bmatrix}n_{22}(t-\tau_2)-n_{22,\text{eq}}\\ n_{21}(t-\tau_2)-n_{21,\text{eq}}\end{bmatrix}\in\mathbb{R}^2,$$

$\Delta n_{11}(t)(\Delta n_{22}(t))$ is the deviation variable from equilibrium of the number of vehicles in region 1 (region 2) with destination to inside the region, $\Delta n_{12}(t)(\Delta n_{21}(t))$ is the deviation variable from equilibrium of the number of vehicles in region 1 (region 2) with destination to region 2 (region 1), the outputs $y_i(t)=\Delta n_i(t)\in\mathbb{R}$ are the deviation variables of the total number of vehicles in region $i=1,2$, and the perimeter control inputs for regions 1, 2 are $u_1(t)=\Delta u_{12}(t)=u_{12}(t)-u_{12,\text{eq}}\in\mathbb{R}$, $u_2(t)=\Delta u_{21}(t)=u_{21}(t)-u_{21,\text{eq}}\in\mathbb{R}$, respectively. The constant system parameter matrices $A_i,\tilde{A}_i,A_{ij},\tilde{A}_{ij}\in\mathbb{R}^{2\times2}$, and $b_i\in\mathbb{R}^{2\times1}$ have *unknown* elements, and τ_i, $i=1,2$, are known time delays.

7.2. Numerical results

In the following numerical examples, except Example 2, it is assumed that both regions have the same MFD, i.e. $\text{MFD}_1=\text{MFD}_2=\text{MFD}_{\text{Yok}}$, where MFD_{Yok} denotes the MFD observed in Yokohama, refer to Geroliminis and Daganzo (2008), with the parameters $n_{\text{cr}}=3400$ (veh), $n_{\max}=10021$ (veh), $G(n_{\text{cr}})=6.3$ (veh/s). Example 2 tests the adaptive perimeter control for different shapes of MFD. The Yokohama MFD is normalized by $n_{\max}$ and $G_{\max}$, e.g. $n_{\text{cr,norm}}=n_{\text{cr}}/n_{\max}=0.34$, as shown in Fig. 5. The traffic flow demands are assumed to be constant with $q_{11}=1.137$, $q_{12}=1.2$, $q_{21}=0.94$, $q_{22}=3.19$, which simulate the case of total demand in region 2 is larger than total demand in region 1, and $\epsilon=0.8$.

A linearized model of the two regions is obtained after linearization around the equilibrium point $(n_{11,\text{eq}},n_{12,\text{eq}},n_{21,\text{eq}},n_{22,\text{eq}},u_{12,\text{eq}},u_{21,\text{eq}})=(1200,2000,1000,2300,0.31,0.49)$. The parameter values of the linearized model (39) are as follows

$$A_1=\begin{bmatrix}-4.1564 & 2.4939\\ 1.2692 & -0.7615\end{bmatrix}\cdot10^{-4},\qquad \tilde{A}_1=\begin{bmatrix}-2.4937 & -2.4937\\ -1.2691 & -1.2691\end{bmatrix}\cdot10^{-4},$$

$$A_{12}=\begin{bmatrix}-2.2927 & -0.9968\\ 0 & 0\end{bmatrix}\cdot10^{-4},\qquad \tilde{A}_{12}=\begin{bmatrix}0.9968 & 0.9968\\ 0 & 0\end{bmatrix}\cdot10^{-4},$$

$$A_2=\begin{bmatrix}-2.2927 & 0.9968\\ 4.635 & -2.015\end{bmatrix}\cdot10^{-4},\qquad \tilde{A}_2=\begin{bmatrix}-0.9968 & -0.9968\\ -4.6348 & -4.6348\end{bmatrix}\cdot10^{-4},$$

$$A_{21}=\begin{bmatrix}0 & 0\\ -0.1269 & 0.0762\end{bmatrix}\cdot10^{-4},\qquad \tilde{A}_{21}=\begin{bmatrix}0 & 0\\ 1.2691 & 1.2691\end{bmatrix}\cdot10^{-4},\tag{40}$$

$$b_1=b_2=\begin{bmatrix}-0.6636\\ -1.3273\end{bmatrix}\cdot10^{-4}.\tag{41}$$

The parameters values of the controllers and the reference models, see (21)–(23) and (17), are chosen as:

$$A_{m1}=A_{m2}=\begin{bmatrix}-0.03 & 0\\ 0 & -0.03\end{bmatrix},\ b_{m1}=b_{m2}=[1\quad 1]^T,\ h_1=h_2=1,\ \Gamma_{11}=0.4I_{4\times4},$$
$$\Gamma_{22}=0.6I_{4\times4},\ \Gamma_{m1}=4\cdot10^6I_{8\times8},\ \Gamma_{m2}=2.5\cdot10^6I_{8\times8},\ \Gamma_{z1}=5\cdot10^6I_{8\times8},$$
$$\Gamma_{z2}=3.5\cdot10^6I_{8\times8},\ g_{d1}=g_{d2}=\text{diag}\{1\quad 1\},\ F_{d1}=F_{d2}=\text{diag}\{-1\quad -1\}.\tag{42}$$

In the following numerical examples, except Example 4, the control objective is to make $n_i(t)$ tends to $n_{mi}(t)(=n_{i,\text{eq}})$ asymptotically. In Example 4, the objective is to track accumulation trajectories which vary with time.

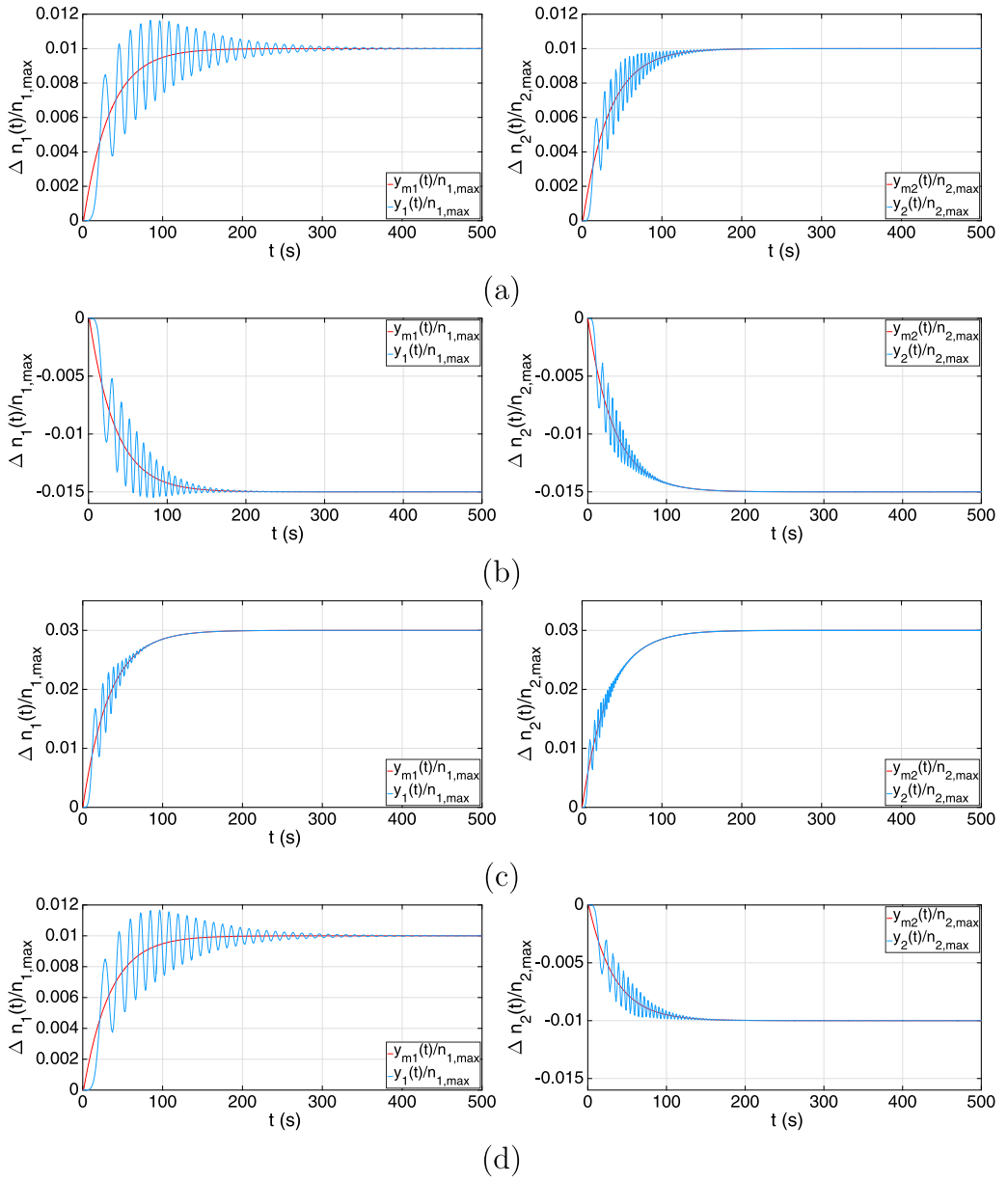

Fig. 6. Example 1– different levels of initial regional accumulations: (a) $\Delta n_1(0) = \Delta n_2(0) = 100$ (veh), (b) $\Delta n_1(0) = \Delta n_2(0) = -150$, (c) $\Delta n_1(0) = \Delta n_2(0) = 300$, and (d) $\Delta n_1(0) = 100$, $\Delta n_2(0) = -100$.

Example 1. In Example 1, we have tested the distributed adaptive perimeter control for different levels of initial regional accumulations. Simulation of the adaptive control for the two-region model with delayed MFD outputs, (39), with the plant coefficients, (40) and (41), are shown in Fig. 6, where the parameters of the controllers are shown in (42). The graphs show the time history of the outputs $\Delta n_1(t)$ (left subplot), $\Delta n_2(t)$ (right subplot) for different initial accumulations: (a) $\Delta n_1(0) = \Delta n_2(0) = 100$ (veh), (b) $\Delta n_1(0) = \Delta n_2(0) = -150$ (veh), (c) $\Delta n_1(0) = \Delta n_2(0) = 300$ (veh), and (d) $\Delta n_1(0) = 100$, $\Delta n_2(0) = -100$ (veh). The corresponding average time delays, according to (4), for: (a) $\Delta n_1(0) = \Delta n_2(0) = 100$ at the equilibrium point $(n_{1,eq}, n_{2,eq}) = (3200, 3300)$ are $\tau_1 = 516$ (s) and $\tau_2 = 532$ (s); (b) $\Delta n_1(0) = \Delta n_2(0) = 150$ at the equilibrium point $(n_{1,eq}, n_{2,eq}) = (3050, 3150)$ are $\tau_1 = 498$ (s) and $\tau_2 = 513$ (s); (c) $\Delta n_1(0) = \Delta n_2(0) = 300$ at the equilibrium point $(n_{1,eq}, n_{2,eq}) = (3200, 3300)$ are $\tau_1 = 532$ (s) and $\tau_2 = 538$ (s); and (d) $\Delta n_1(0) = \Delta n_2(0) = 150$ at the equilibrium point $(n_{1,eq}, n_{2,eq}) = (3200, 3150)$ are $\tau_1 = 520$ (s) and $\tau_2 = 513$ (s).

The results verify the performance efficiency of the adaptive perimeter control for different initial accumulations.

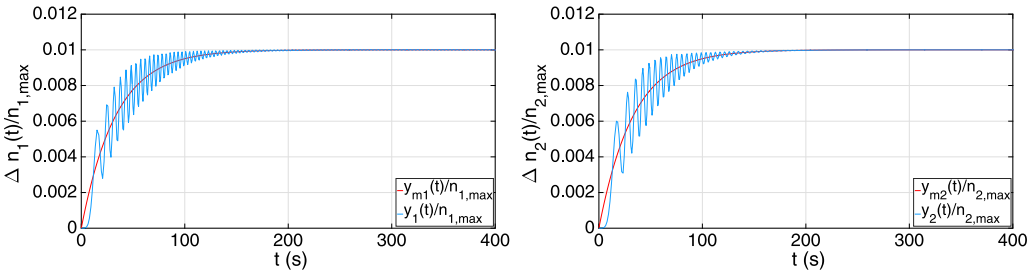

Fig. 7. Example 2– different MFDs for regions 1 and 2, i.e. $\text{MFD}_1 = 1.2\text{MFD}_{\text{Yok}}$ and $\text{MFD}_2 = 0.8\text{MFD}_{\text{Yok}}$.

Example 2. In Example 2, we have examined the same adaptive control (18)–(20) with adaptation gain rules from (21)–(23) (without retuning), with the same structure of the reference model (17), to different matrices of parameters of the system, i.e. different shapes of MFDs.

The performance of the adaptive perimeter control for the two urban regions with different MFDs, i.e. $\text{MFD}_1 = 1.2\text{MFD}_{\text{Yok}}$ and $\text{MFD}_2 = 0.8\text{MFD}_{\text{Yok}}$ see Fig. 5, is evaluated as shown in Fig. 7. The equilibrium points for both regions are kept the same, i.e. $n_{1,\text{eq}} = 3200$, $n_{2,\text{eq}} = 3300$ (veh). The corresponding average time delays at these equilibrium points for $\Delta n_1(t) = \Delta n_2(t) = 100$ are $\tau_1 = 443$ (s) and $\tau_2 = 665$ (s).

The results in Fig. 7 show that the desired performance is met for the two urban regions with different sizes of MFDs. The results demonstrate the possibilities of the adaptive control scheme for two regions under incompletely specified MFD plant models.

Example 3. In Example 3, we demonstrate the importance of coordination by changing the relative weight between local information and coordination. This is done by changing the parameters Γ_{mi} and Γ_{zi} in (22) and (23), while keeping the other parameters unchanged.

The control parameters Γ_{mi} and Γ_{zi} in (22) and (23) are related to the coordination part of the controllers. These parameters are tuned and tested for several values: (a) base values taken from (42), (b) both parameters are decreased by multiplying base values by 0.1, (c) both parameters are increased by multiplying base values by 10, and (d) Γ_{m1} and Γ_{z1} are increased by multiplying base values by 10, while Γ_{m2} and Γ_{z2} are decreased by multiplying base values by 0.1. As it can be observed from the results in Fig. 8, increasing the parameter values increases the weight of the coordination information, which result a better performance of the transient behavior.

Example 4. Note that the accumulation references in examples 1,2,3 are a priori given constant accumulation points. In Example 4, the adaptive perimeter control is tested for time varying accumulation references: (a) a square wave for region 1 and (b) a sine wave for region 2, with amplitudes 100 (veh). The corresponding average time delays at the equilibrium point $n_{1,\text{eq}} = 3100$, $n_{2,\text{eq}} = 3200$ (veh) for square and sine functions with amplitudes 100 are respectively $\tau_1 = 509$ (s) and $\tau_2 = 524$ (s). The output signal y_i and the output of reference model $y_{m,i}$, i.e. time varying accumulation references, are shown in Fig. 9. The simulation results show the effectiveness of the adaptive control in tracking the reference models with time varying accumulations.

Example 5. Finally, in Example 5, we examine the effect of integrating the delay in the reference control model. In this example, we consider the plant model of Example 1(a) with delays τ_1 and τ_2, and examine the adaptive perimeter control for two cases: (a) with reference models without delays, and (b) with reference models with delays, same values of the plant delays. The results are shown in Fig. 10. The results show that in both cases the adaptive control performs well, as the plant accumulations track the reference accumulations. However, note that the transient behaviors are different.

8. Numerical example: adaptive perimeter control with delayed interconnections for three urban regions

In this section, results of a numerical example are presented to explore the features of the adaptive perimeter control II, i.e. (18), (30), (38), for an MFD system of three regions with delayed interconnections, see (25) and (26). The dynamic equations for the three-region system are explicitly written in (B.1)–(B.3).

8.1. Linearized three-region model for adaptive perimeter control design

According to (29), the linearized state space model for the three-region system with delayed interconnections can be written as,

$$\begin{aligned}
\dot{x}_1(t) &= A_1 x_1(t) + B_1 u_1(t) + \tilde{A}_{21}\tilde{x}_2(t-\tau_2) + \tilde{A}_{31}\tilde{x}_3(t-\tau_3)\,,\\
\dot{x}_2(t) &= A_2 x_2(t) + B_2 u_2(t) + \tilde{A}_{12}\tilde{x}_1(t-\tau_1) + \tilde{A}_{32}\tilde{x}_3(t-\tau_3)\,,\\
\dot{x}_3(t) &= A_3 x_3(t) + B_3 u_3(t) + \tilde{A}_{13}\tilde{x}_1(t-\tau_1) + \tilde{A}_{23}\tilde{x}_2(t-\tau_2)\,,
\end{aligned} \tag{43}$$

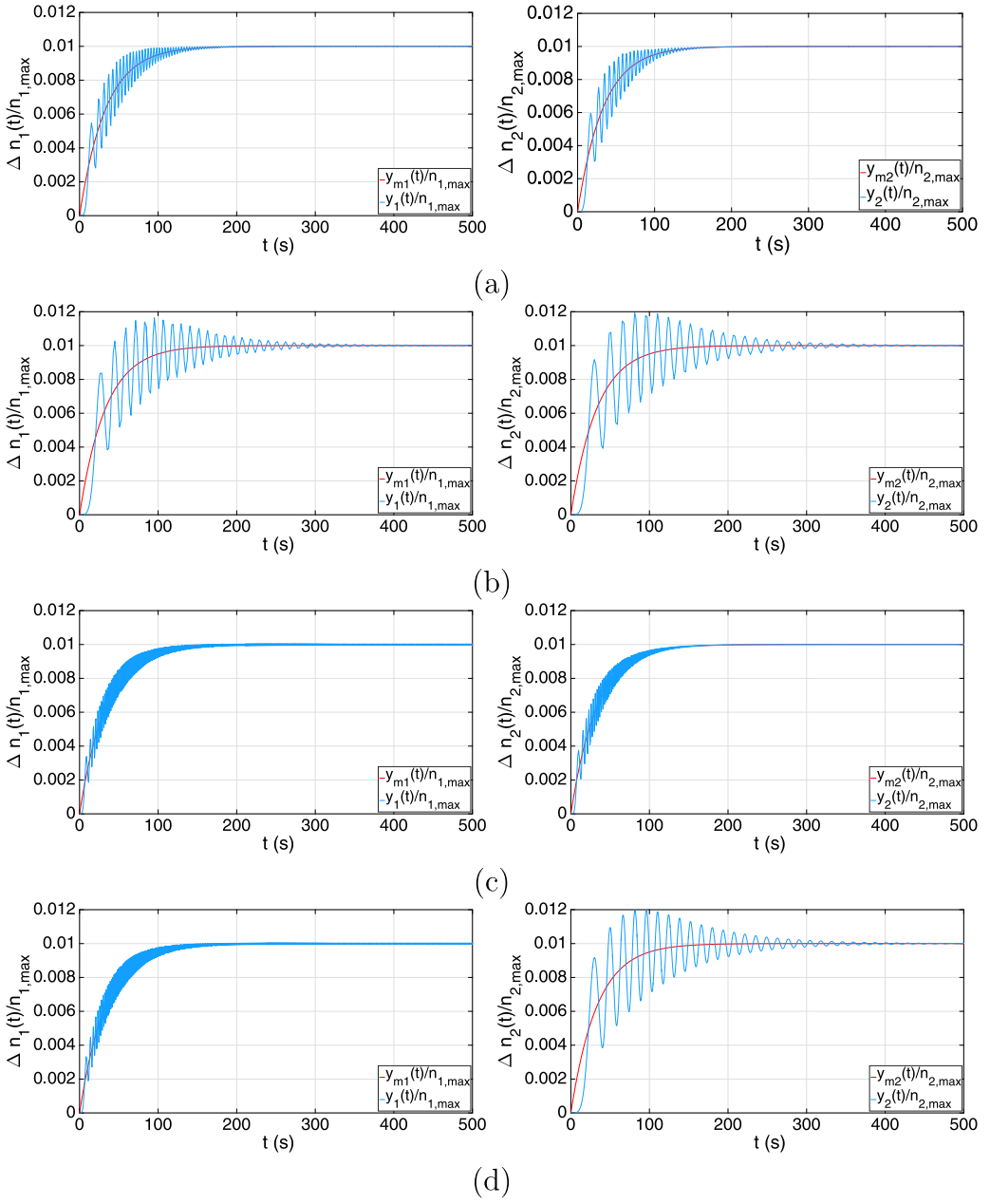

Fig. 8. Example 3– effect of coordination gain parameters in the perimeter control: (a) base values of Γ_{mi} and Γ_{zi} taken from (42), (b) 0.1 × base values, (c) 10 × base values, (d) 10 × base values for Γ_{m1} and Γ_{z1}, and 0.1 × base values for Γ_{m2} and Γ_{z2}.

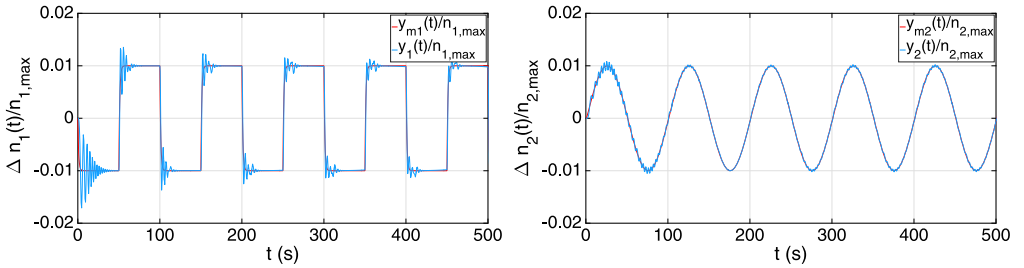

Fig. 9. Example 4– time varying accumulation references: (a) a square wave for region 1, and (b) a sine wave for region 2, with amplitudes 100 (veh).

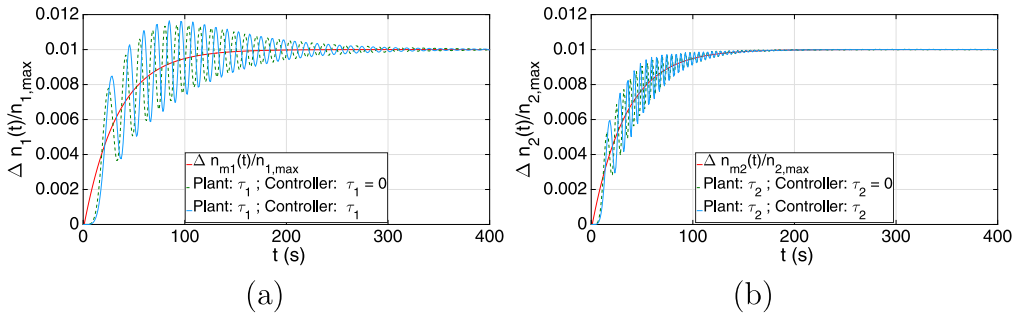

Fig. 10. Example 5– Plant model with delays, while the adaptive control with (a) reference models without delays, and with (b) reference models with delays, same values of the plant delays.

where

$$x_1(t)=\begin{bmatrix}\Delta n_{11}(t)\\ \Delta n_{12}(t)\\ \Delta n_{13}(t)\end{bmatrix},\quad x_2(t)=\begin{bmatrix}\Delta n_{22}(t)\\ \Delta n_{21}(t)\\ \Delta n_{23}(t)\end{bmatrix},\quad x_3(t)=\begin{bmatrix}\Delta n_{33}(t)\\ \Delta n_{31}(t)\\ \Delta n_{32}(t)\end{bmatrix},$$

$$\tilde{x}_1(t)=\begin{bmatrix}\Delta n_{11}(t-\tau_1)\\ \Delta n_{12}(t-\tau_1)\\ \Delta n_{13}(t-\tau_1)\end{bmatrix},\quad \tilde{x}_2(t)=\begin{bmatrix}\Delta n_{22}(t-\tau_2)\\ \Delta n_{21}(t-\tau_2)\\ \Delta n_{23}(t-\tau_2)\end{bmatrix},\quad \tilde{x}_3(t)=\begin{bmatrix}\Delta n_{33}(t-\tau_3)\\ \Delta n_{31}(t-\tau_3)\\ \Delta n_{32}(t-\tau_3)\end{bmatrix},$$

$$u_1(t)=\begin{bmatrix}\Delta u_{11}(t)\\ \Delta n_{12}(t)\\ \Delta n_{13}(t)\end{bmatrix},\quad u_2(t)=\begin{bmatrix}\Delta u_{22}(t)\\ \Delta u_{21}(t)\\ \Delta u_{23}(t)\end{bmatrix},\quad u_3(t)=\begin{bmatrix}\Delta u_{33}(t)\\ \Delta u_{31}(t)\\ \Delta u_{32}(t)\end{bmatrix},$$

with $\Delta n_{ij}(t)=n_{ij}(t)-n_{ij,\text{eq}}$, $\Delta n_{ij}(t-\tau_i)=n_{ij}(t-\tau_i)-n_{ij,\text{eq}}$, and $\Delta u_{ij}(t)=u_{ij}(t)-u_{ij,\text{eq}}$.

8.2. Numerical results

In Example 6, it is assumed that all regions have the same MFD, i.e. $\text{MFD}_1=\text{MFD}_2=\text{MFD}_3=\text{MFD}_{\text{Yok}}$. The interconnection time delays are assumed to be constant $\tau_1=6\,(\text{s})$, $\tau_2=5\,(\text{s})$, and $\tau_3=10\,(\text{s})$.

A linearized MFD-based model of the three regions is obtained at the equilibrium point for region 1: $n_{11,\text{eq}}=1200$, $n_{12,\text{eq}}=800$, $n_{13,\text{eq}}=1000$, $q_{11,\text{eq}}=0.695$, $q_{12,\text{eq}}=0.5$, $q_{13,\text{eq}}=0.6$, $u_{12,\text{eq}}=0.3$, $u_{13,\text{eq}}=0.288$, and for region 2: $n_{21,\text{eq}}=700$, $n_{22,\text{eq}}=1300$, $n_{23,\text{eq}}=1200$, $q_{21,\text{eq}}=0.7$, $q_{22,\text{eq}}=1.15$, $q_{23,\text{eq}}=0.8$, $u_{21,\text{eq}}=0.509$ $u_{23,\text{eq}}=0.339$, and for region 3: $n_{31,\text{eq}}=900$, $n_{32,\text{eq}}=1000$, $n_{33,\text{eq}}=1200$, $q_{31,\text{eq}}=1.1$, $q_{32,\text{eq}}=0.9$, $q_{33,\text{eq}}=1.026$, $u_{31,\text{eq}}=0.605$, $u_{32,\text{eq}}=0.445$. Given these equilibrium values, the parameter values of the linearized model (43) are as follows:

Region 1:

$$A_1=\begin{bmatrix}-1.3830 & 0.6962 & 0.6962\\ 0.1395 & -0.4854 & 0.1395\\ 0.1674 & 0.1674 & -0.4325\end{bmatrix}\cdot 10^{-3},\tilde{A}_{21}=\begin{bmatrix}0.7991 & -0.2008 & -0.2008\\ 0 & 0 & 0\\ 0 & 0 & 0\end{bmatrix}\cdot 10^{-3}$$

$$\tilde{A}_{31}=\begin{bmatrix}0.9110 & -0.3112 & -0.3112\\ 0 & 0 & 0\\ 0 & 0 & 0\end{bmatrix}\cdot 10^{-3},B_1=\begin{bmatrix}1 & 0 & 0\\ 0 & -1.6634 & 0\\ 0 & 0 & -2.0793\end{bmatrix},\tag{44}$$

Region 2:

$$A_2=\begin{bmatrix}-0.7991 & 0.2008 & 0.2008\\ 0.7328 & -1.2321 & 0.7328\\ 0.2295 & 0.2295 & -0.4371\end{bmatrix}\cdot 10^{-3},\tilde{A}_{12}=\begin{bmatrix}0 & 0 & 0\\ -0.1395 & 0.4854 & -0.1395\\ 0 & 0 & 0\end{bmatrix}\cdot 10^{-3}$$

$$\tilde{A}_{32}=\begin{bmatrix}0 & 0 & 0\\ -0.2546 & 0.6453 & -0.2546\\ 0 & 0 & 0\end{bmatrix}\cdot 10^{-3},B_2=\begin{bmatrix}-1.3754 & 0 & 0\\ 0 & 1 & 0\\ 0 & 0 & -2.3579\end{bmatrix},\tag{45}$$

Region 3:

$$A_3=\begin{bmatrix}-0.9110 & 0.3112 & 0.3112\\ 0.2546 & -0.6453 & 0.2546\\ 0.6863 & 0.6863 & -1.3353\end{bmatrix}\cdot 10^{-3},\tilde{A}_{13}=\begin{bmatrix}0 & 0 & 0\\ 0 & 0 & 0\\ -0.1674 & -0.1674 & 0.4325\end{bmatrix}\cdot 10^{-3}$$

$$\tilde{A}_{23}=\begin{bmatrix}0 & 0 & 0\\ 0 & 0 & 0\\ -0.2295 & -0.2295 & 0.4371\end{bmatrix}\cdot 10^{-3}, B_3=\begin{bmatrix}-1.8195 & 0 & 0\\ 0 & -2.0217 & 0\\ 0 & 0 & 1\end{bmatrix}, \tag{46}$$

According to the controller structure (18), with $u_{li}(t)$ from (30) and $u_{ci}(t)$ from (33), in the case of three regions system, the controller of region 1, for example, is given as

$$u_1(t)=\theta_{l1}^{\mathrm{T}}\omega_{l1}(t)+\theta_{12}^{\mathrm{T}}\omega_{12}(t)+\theta_{13}^{\mathrm{T}}\omega_{13}(t), \tag{47}$$

where

$$\begin{aligned}
\omega_{l1}(t)&=\begin{bmatrix}e_{11}(t) & e_{12}(t) & e_{13}(t) & r_{11}(t) & r_{12}(t) & r_{13}(t) & x_{r11}(t) & x_{r12}(t) & x_{r13}(t)\end{bmatrix}^{\mathrm{T}},\\
\omega_{12}(t)&=\begin{bmatrix}x_{r21}(t-\tau_2) & x_{r22}(t-\tau_2) & x_{r23}(t-\tau_2)\end{bmatrix}^{\mathrm{T}},\\
\omega_{13}(t)&=\begin{bmatrix}x_{r31}(t-\tau_3) & x_{r32}(t-\tau_3) & x_{r33}(t-\tau_3)\end{bmatrix}^{\mathrm{T}},\\
\theta_{l1}^{\mathrm{T}}(t)&=-\gamma_{11}S_{p1}\mathrm{PITD}(e_1(t)\omega_{l1}^{\mathrm{T}}(t)),\\
\theta_{12}^{\mathrm{T}}(t)&=-\gamma_{12}S_{p1}\mathrm{PITD}(e_1(t)\omega_{12}^{\mathrm{T}}(t)),\\
\theta_{13}^{\mathrm{T}}(t)&=-\gamma_{13}S_{p1}\mathrm{PITD}(e_1(t)\omega_{13}^{\mathrm{T}}(t)),
\end{aligned} \tag{48}$$

with $e_{11}(t)=x_{11}(t)-x_{r11}(t)$, $e_{12}(t)=x_{12}(t)-x_{r12}(t)$, $e_{13}(t)=x_{13}(t)-x_{r13}(t)$, $\mathrm{PITD}(x_i(t))=k_{\mathrm{I}}\int_0^t x_i(s)\mathrm{d}s+k_{\mathrm{P}}x_i(t)+k_{\mathrm{D}}x_i(t-h_i), i=1,2$. k_{I}, k_{P}, k_{D} are known tuning coefficients. Note that this adaptation algorithm is exactly the same adaptation algorithm presented in (38), but it is re-written here differently.

The parameters of the adaptation in (48) and the reference model coefficients are chosen as

$$\begin{aligned}
&A_{r1}=A_{r2}=A_{r3}=\begin{bmatrix}-1 & 0 & 0\\ 0 & -1 & 0\\ 0 & 0 & -1\end{bmatrix}, B_{r1}=B_{r2}=B_{r3}=[1\quad 1\quad 1]^{\mathrm{T}},\\
&\tau_1=6,\tau_2=5,\tau_3=10,\\
&S_{pi}=\begin{bmatrix}1 & -1 & -1\\ -1 & -1 & -1\\ -1 & -1 & -1\end{bmatrix}\cdot 10^{-3},\\
&\gamma_{11}=-0.5,\gamma_{12}=1.89,\gamma_{13}=1,\gamma_{21}=1.5,\gamma_{22}=3.8,\gamma_{23}=1.8,\\
&\gamma_{31}=1,\gamma_{32}=5,\gamma_{33}=10,h_1=h_2=h_3=1,\\
&K_I=0.05,\ K_P=4,K_D=0.005\,.
\end{aligned} \tag{49}$$

In Example 6, we have tested distributed adaptive perimeter control for different types of reference for regional accumulations. I.e. for region 1: varying accumulation reference $n_{11}(t)$ with input signal $12\sin(2\pi/5\cdot t)$, a step function at time $t=0$ for n_{12}, and a step function at time $t=5$ for n_{12}; for regions 2 and 3: the reference accumulations are step functions at $t=5$ with $\Delta n_{21}=\Delta n_{22}=\Delta n_{23}=\Delta n_{31}=\Delta n_{32}=\Delta n_{33}=30$. The results, shown in Fig. 11, also verify the efficient performance of the adaptive control, as the outputs track the reference signals. The proposed distributed adaptive control based on the MFD model with delayed interconnections perform well.

9. Conclusions, discussion, and future research

In this paper, two enhanced nonlinear accumulation-based models with state delays for urban regions were developed. The first model incorporates state delay in the MFD output to improve the dynamics, while in the second model delayed interconnections are introduced in the dynamic equations to model data processing and communication delays between interconnected regions. The reference model adaptive control (MRAC) approach has been implemented to design distributed adaptive perimeter control laws. The developed adaptive control scheme postulates one controller structure. The controllers' gains vary with time to adapt themselves against the model parameter uncertainties and state delays.

The adaptive controllers were shown to be efficient for different conditions by numerical examples. The results show that the distributed adaptive perimeter controllers can bring different initial accumulations to equilibrium accumulations, and can perform well for different shapes of MFDs in case of uncertainties in MFDs. Moreover, the numerical results show that for multi-region systems with state delays, the adaptive controllers are capable to stabilize the regional accumulations at the a priori given constant equilibrium points, and also can be utilized for arbitrary time-varying desired behavior. In all numerical examples, it was shown that the desired tracking performance is met. The results demonstrate the flexibility of the distributed adaptive perimeter controllers in handling different cases and various traffic situations with state delays.

The contribution of this paper does not only enhance the MFD modeling, but it also improves the perimeter control algorithms. As shown, the current control scheme is general and can be applied for multiple regions.

In this paper, our modeling approach is to incorporate time delays to better describe wave propagation and travel time evolution within the region. The idea is that the complex dynamics can be approximated by relatively simple dynamics and

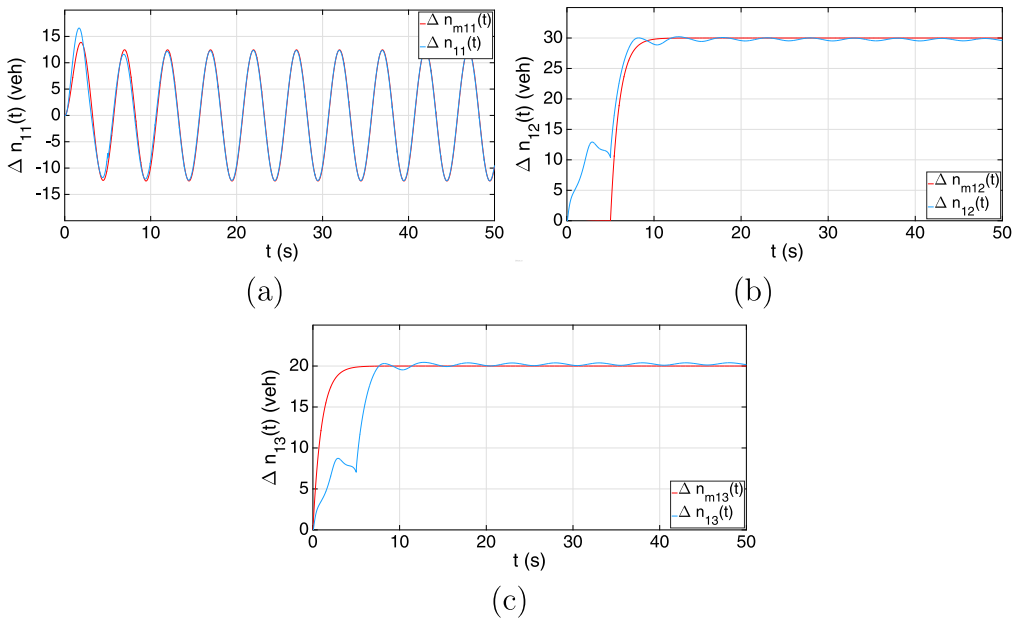

Fig. 11. Example 6 – delayed interconnections for the three-region system with (a) varying accumulation reference $n_{11}(t)$, (b) a step function at time $t = 0$ for n_{12}, and (c) a step function at time $t = 5$ for n_{12}.

a delay part. This allows us to utilize accumulation-based models but with state delays, which add extra information (or "memory") related to reaction times. Another modeling approach was presented in recent works (Arnott, 2013; Fosgerau, 2015; Lamotte and Geroliminis, 2016; Mariotte et al., 2017), as trip-based MFD models have been developed to consider variable trip lengths in single-region dynamics. Future research should focus on analyzing and comparing between trip-based models and accumulation-based models, *but* with state delays, for multi-region systems. Note that very interesting comparison results have been obtained in Mariotte et al. (2017) between trip-based and accumulation-based without state delays for single-region dynamics. Another future research should focus on developing perimeter control strategies for trip-based models. Comparison between these strategies and control strategies developed in this paper, based on accumulation-based models with state delays, is another future research. The comparison should consider different aspects, not only performance, but also implementation and application issues.

Note that the delays are considered constant only during the current time step of calculations. This means that at each time step, new value of "constant" delay can be calculated. In other words, in case of considering varying time delay, it can be approximated by piecewise constant values, i.e. constant delays during each time step of calculation. Hence, the current work can also handle time delays which change over time, since the procedure can be recalculated each time step according to the new equations presented in the current paper.

The current algorithms do not handle control input constraints, e.g. lower and upper bounds. In the numerical examples, these constraints were taken into account by truncating the control inputs if they violate the constraints. Even though in all presented examples truncating the control inputs did not affect the stability, future research might focus on integrating control and/or state constraints into the presented control algorithms, by imposing them within the control design in a systematic way. This is very important to ensure the controller law feasibility and stability of the system for a more realistic scenarios. Recent preliminarily results on integrating control constraints into a perimeter control algorithm designed by MRAC, but for other dynamics, have been reported in Haddad and Mirkin (2016a). A future research might focus on developing the current algorithms presented in this paper for the accumulation-based models with state delays, based on the results of MARC with constraints presented in Haddad and Mirkin (2016a).

One of the reviewers of this paper mentioned that the transfer flows from an origin region to a destination region might affect intermediate regions, and hence, transfer flows with *time delays* should be also incorporated in aggregated models. This indeed might be a relevant issue for an accumulation-based model with route choice modeling, e.g. as was developed in Yildirimoglu et al. (2015). We believe that the current model approach can be further developed to incorporate such delays in aggregate models that take into account route choice and intermediate regions. This would be a future research topic.

The adaptive perimeter control algorithms presented in this paper were developed based on the adaptive algorithms presented in Mirkin and Gutman (2003, 2005). The adaptive algorithms were proved to guarantee closed-loop stability and also asymptotic zero tracking errors, when uncertainties and delays are present in the subsystems and interconnections. It should be stressed that stability and tracking were proven for linear plants. Clearly, if the adaptive algorithms are applied

to nonlinear plants, then we might have issues with guaranteeing stability. In this paper, the adaptive perimeter controllers were designed and applied for linear plants. The reported results show that the closed-loop stability and asymptotic zero tracking errors are obtained. However, when the designed perimeter algorithms were applied for the original nonlinear plant model, non-desirable performances were observed in few numerical cases. Hence, some performance issues might appear when they are applied to real traffic network and/or microsimulation test studies, if the linear plants do not replicate the nonlinear dynamics, e.g. during congested regimes while the MFD is operated on the decreasing part of the MFD. One approach to tackle this problem is to incorporate higher-order terms after linearization, i.e. residual approximation errors inherent in the linear parameterization of the system uncertainty, and an unknown dynamics offset introduced by the non-equilibrium operating points, to the linear plant model. More efforts and future research should focus on dealing with this issue before real implementations.

One of the reviewers comments that some results of the numerical examples obtained "large oscillations" during the transient phase. It should be noted that the main goals of the presented numerical examples were to examine the stability of the adaptive algorithms, to analyze the effect of the algorithm parameters, and to evaluate the performance for several scenarios. It should be stressed that tuning process for some constant algorithm parameters, e.g. coordination gain parameters, could further improve the transient performance, see e.g. Example 3 and Fig. 8.

As said above, utilizing the adaptive control algorithms guarantee asymptotic zero tracking errors. However, it is more difficult to control the transient reaction period. This might not be an important issue, if the considered problem is a mathematical problem without a physical meaning, however, dealing with a traffic control problem, some transient specifications should be guaranteed as well. Future research should also determine and define such transient specifications for perimeter control problems.

Towards real applications, utilizing other approaches to develop other perimeter control strategies are very recommended. To the best of our knowledge, current perimeter control strategies in the literature should be modified to deal with the new introduced multi-region accumulation-based models with state delays. This would shed some light on the advantages and disadvantages of the MRAC approach implemented in the current paper, and which control approach, and in which traffic conditions, is better to use for real application. This also should be a future research.

Future research might utilize the developed models in this paper for other MFD-based control problems, with or without perimeter control, for route guidance strategies. Integrating interconnection delays is considered as a one step forward towards realistic accumulation-based modeling and real practical perimeter control implementation. Future research should also focus on other real application-oriented problems.

Acknowledgments

This research was supported by the Israel Science Foundation (ISF Grant No. 0251502). This research was financially supported by the Technion. The research leading to these results has received funding from the European Union's - Seventh Framework Programme (FP7/2007-2013) under grant agreement n° 630690-MC–SMART.

Appendix A. Nonlinear two-region model with delayed MFD outputs

The vehicle conservation equations for two urban regions with delayed MFD outputs are formulated as follows, see (13)–(15) and (5),

$$\frac{dn_{11}(t)}{dt} = q_{11}(t) + u_{21}(t)\cdot\frac{n_{21}(t)}{n_2(t)}\cdot G_2(n_2(t-\tau_2)) - \frac{n_{11}(t)}{n_1(t)}\cdot G_1(n_1(t-\tau_1))\,, \tag{A.1}$$

$$\frac{dn_{12}(t)}{dt} = q_{12}(t) - u_{12}(t)\cdot\frac{n_{12}(t)}{n_1(t)}\cdot G_1(n_1(t-\tau_1))\,, \tag{A.2}$$

$$\frac{dn_{21}(t)}{dt} = q_{21}(t) - u_{21}(t)\cdot\frac{n_{21}(t)}{n_2(t)}\cdot G_2(n_2(t-\tau_2))\,, \tag{A.3}$$

$$\frac{dn_{22}(t)}{dt} = q_{22}(t) + u_{12}(t)\cdot\frac{n_{12}(t)}{n_1(t)}\cdot G_1(n_1(t-\tau_1)) - \frac{n_{22}(t)}{n_2(t)}\cdot G_2(n_2(t-\tau_2))\,, \tag{A.4}$$

$$n_1(t-\tau_1) = n_{11}(t-\tau_1) + n_{12}(t-\tau_1)\,, \tag{A.5}$$

$$n_2(t-\tau_2) = n_{11}(t-\tau_2) + n_{12}(t-\tau_2)\,, \tag{A.6}$$

$$n_1(t) = n_{11}(t) + n_{12}(t)\,, \tag{A.7}$$

$$n_2(t) = n_{21}(t) + n_{22}(t)\,. \tag{A.8}$$

where $q_{11}(t)$ (veh/s) and $q_{22}(t)$ (veh/s) are the two endogenous traffic demands in R_1 and R_2, respectively, $n_{12}(t)$(veh) ($n_{21}(t)$(veh)) us the number of vehicles in region 1 (2) with destination to region 2 (1) at time t. $n_1(t)$ (veh) ($n_2(t)$) is the accumulation or the total number of vehicles in region 1 (2) at time t, i.e. $n_i(t) = \sum_j n_{ij}(t)$.

Appendix B. Nonlinear three-region model with delayed interconnections

The dynamic equations for the three-region system with delayed interconnections are given as follows

$$\begin{aligned}
\dot{n}_{11}(t) &= q_{11}(t) + \frac{n_{21}(t-\tau_2)}{n_2(t-\tau_2)} \cdot G_2(n_2(t-\tau_2)) \cdot u_{21}(t) \\
&\quad + \frac{n_{31}(t-\tau_3)}{n_3(t-\tau_3)} \cdot G_3(n_3(t-\tau_3)) \cdot u_{31}(t) - \frac{n_{11}(t)}{n_1(t)} \cdot G_1(n_1(t)), \\
\dot{n}_{12}(t) &= q_{12}(t) - \frac{n_{12}(t)}{n_1(t)} \cdot G_1(n_1(t)) \cdot u_{12}(t), \\
\dot{n}_{13}(t) &= q_{13}(t) - \frac{n_{13}(t)}{n_1(t)} \cdot G_1(n_1(t)) \cdot u_{13}(t),
\end{aligned} \tag{B.1}$$

$$\begin{aligned}
\dot{n}_{21}(t) &= q_{21}(t) - \frac{n_{21}(t)}{n_2(t)} \cdot G_2(n_2(t)) \cdot u_{21}(t), \\
\dot{n}_{22}(t) &= q_{22}(t) + \frac{n_{12}(t-\tau_1)}{n_1(t-\tau_1)} \cdot G_1(n_1(t-\tau_1)) \cdot u_{12}(t) \\
&\quad + \frac{n_{32}(t-\tau_3)}{n_3(t-\tau_3)} \cdot G_3(n_3(t-\tau_3)) \cdot u_{32}(t) - \frac{n_{22}(t)}{n_2(t)} \cdot G_2(n_2(t)), \\
\dot{n}_{23}(t) &= q_{23}(t) - \frac{n_{23}(t)}{n_2(t)} \cdot G_2(n_2(t)) \cdot u_{23}(t),
\end{aligned} \tag{B.2}$$

$$\begin{aligned}
\dot{n}_{31}(t) &= q_{31}(t) - \frac{n_{31}(t)}{n_3(t)} \cdot G_3(n_3(t)) \cdot u_{31}(t), \\
\dot{n}_{32}(t) &= q_{32}(t) - \frac{n_{32}(t)}{n_3(t)} \cdot G_3(n_3(t)) \cdot u_{32}(t), \\
\dot{n}_{33}(t) &= q_{33}(t) + \frac{n_{13}(t-\tau_1)}{n_1(t-\tau_1)} \cdot G_1(n_1(t-\tau_1)) \cdot u_{13}(t) \\
&\quad + \frac{n_{23}(t-\tau_2)}{n_2(t-\tau_2)} \cdot G_2(n_2(t-\tau_2)) \cdot u_{23}(t) - \frac{n_{33}(t)}{n_3(t)} \cdot G_3(n_3(t)).
\end{aligned} \tag{B.3}$$

References

Aboudolas, K., Geroliminis, N., 2013. Perimeter and boundary flow control in multi-reservoir heterogeneous networks. Transp. Res. Part B 55, 265–281.
Arnott, R., 2013. A bathtub model of downtown traffic congestion. J. Urban Econ. 76, 110–121.
Buisson, C., Ladier, C., 2009. Exploring the impact of homogeneity of traffic measurements on the existence of macroscopic fundamental diagrams. Transp. Res. Rec. 2124, 127–136.
Daganzo, C.F., 2007. Urban gridlock: macroscopic modeling and mitigation approaches. Transp. Res. Part B 41 (1), 49–62.
Daganzo, C.F., Gayah, V.V., Gonzales, E.J., 2011. Macroscopic relations of urban traffic variables: bifurcations, multivaluedness and instability. Transp. Res. Part B 45 (1), 278–288.
Fosgerau, M., 2015. Congestion in the bathtub. Econ. Transp. 4 (4), 241–255.
Fridman, E., 2014. Introduction to Time-Delay Systems: Analysis and Control. Springer.
Gayah, V.V., Daganzo, C.F., 2011. Clockwise hysteresis loops in the macroscopic fundamental diagram: an effect of network instability. Transp. Res. Part B 45 (4), 643–655.
Geroliminis, N., 2015. Cruising-for-parking in congested cities with an MFD representation. Econ. Transp. 4 (3), 156–165.
Geroliminis, N., Daganzo, C.F., 2008. Existence of urban-scale macroscopic fundamental diagrams: some experimental findings. Transp. Res. Part B 42 (9), 759–770.
Geroliminis, N., Haddad, J., Ramezani, M., 2013. Optimal perimeter control for two urban regions with macroscopic fundamental diagrams: a model predictive approach. IEEE Trans. Intell. Transp. Syst. 14 (1), 348–359.
Geroliminis, N., Sun, J., 2011a. Hysteresis phenomena of a macroscopic fundamental diagram in freeway networks. Transp. Res. Part A 45 (9), 966–979.
Geroliminis, N., Sun, J., 2011b. Properties of a well-defined macroscopic fundamental diagram for urban traffic. Transp. Res. Part B 45 (3), 605–617.
Godfrey, J.W., 1969. Traffic Eng. Control 11 (7), 323–327.
Gu, K., Chen, J., Kharitonov, V.L., 2003. Stability of Time-Delay Systems. Springer Science & Business Media.
Gudin, R., Mirkin, L., 2007. On the delay margin of dead-time compensators. Int. J. Control 80 (8), 1316–1332.
Haddad, J., 2015. Robust constrained control of uncertain macroscopic fundamental diagram networks. Transp. Res. Part C 59, 323–339.
Haddad, J., 2017. Optimal perimeter control synthesis for two urban regions with aggregate boundary queue dynamics. Transp. Res. Part B 96, 1–25.
Haddad, J., Geroliminis, N., 2012. On the stability of traffic perimeter control in two-region urban cities. Transp. Res. Part B 46 (1), 1159–1176.

Haddad, J., Mirkin, B., 2016. Adaptive multiple input delays compensation under input constraints applied to perimeter traffic control. IFAC-Pap. 49 (3), 141–146.
Haddad, J., Mirkin, B., 2016. Adaptive perimeter traffic control of urban road networks based on MFD model with time delays. Int. J. Nonlinear Robust Control 26 (6), 1267–1285. (Special Issue on “Recent Trends in Traffic Modelling and Control”).
Haddad, J., Mirkin, B., 2017. Coordinated distributed adaptive perimeter control for large-scale urban road networks. Transp. Res. Part C 77, 495–515.
Haddad, J., Shraiber, A., 2014. Robust perimeter control design for an urban region. Transp. Res. Part B 68, 315–332.
Hespanha, J.P., Naghshtabrizi, P., Xu, Y., 2007. A survey of recent results in networked control systems. Proc. IEEE 95 (1), 138–162.
Ji, Y., Daamen, W., Hoogendoorn, S., Hoogendoorn-Lanser, S., Qian, X., 2010. Macroscopic fundamental diagram: investigating its shape using simulation data. Transp. Res. Rec. 2161, 42–48.
Ji, Y., Geroliminis, N., 2012. On the spatial partitioning of urban transportation networks. Transp. Res. Part B 46 (10), 1639–1656.
Keyvan-Ekbatani, M., Kouvelas, A., Papamichail, I., Papageorgiou, M., 2012. Exploiting the fundamental diagram of urban networks for feedback-based gating. Transp. Res. Part B 46 (10), 1393–1403.
Keyvan-Ekbatani, M., Papageorgiou, M., Knoop, V., 2015. Controller design for gating traffic control in presence of time-delay in urban road networks. Transp. Res. Part C 59, 308–322.
Keyvan-Ekbatani, M., Papageorgiou, M., Papamichail, I., 2013. Urban congestion gating control based on reduced operational network fundamental diagrams. Transp. Res. Part C 33, 74–87.
Knoop, V.L., Hoogendoorn, S.P., Van Lint, J.W.C., 2012. Routing strategies based on the macroscopic fundamental diagram. Transp. Res. Rec. 2315, 1–10.
Kouvelas, A., Saeedmanesh, M., Geroliminis, N., 2017. Enhancing model-based feedback perimeter control with data-driven online adaptive optimization. Transp. Res. Part B Methodol. 96, 26–45.
Lamotte, R., Geroliminis, N., 2016. The morning commute in urban areas: insights from theory and simulation. Transportation Research Board Annual Meeting. Washington, DC.
Laval, J.A., Castrillón, F., 2015. Stochastic approximations for the macroscopic fundamental diagram of urban networks. Transp. Res. Part B 81, 904–916.
Leclercq, L., Chiabaut, N., Trinquier, B., 2014. Macroscopic fundamental diagrams: a cross-comparison of estimation methods. Transp. Res. Part B 1–12.
Leclercq, L., Parzani, C., Knoop, V.L., Amourette, J., Hoogendoorn, S., 2015. Macroscopic traffic dynamics with heterogeneous route patterns. Transp. Res. Part C 59, 292–307.
Mahmassani, H., Williams, J., Herman, R., 1987. Performance of urban traffic networks. In: Gartner, N., Wilson, N. (Eds.), Proceedings of the Tenth International Symposium on Transportation and Traffic Theory. Elsevier, Amsterdam, The Netherlands.
Mahmassani, H.S., Saberi, M., Zockaie, A.K., 2013. Urban network gridlock: theory, characteristics, and dynamics. Transp. Res. Part C 36, 480–497.
Mariotte, G., Leclercq, L., Laval, J.A., 2017. Macroscopic urban dynamics: analytical and numerical comparisons of existing models. Transp. Res. Part B 101, 245–267.
Marshall, J.E., 1992. Time-delay Systems: Stability and Performance Criteria with Applications. Prentice Hall.
Mazloumian, A., Geroliminis, N., Helbing, D., 2010. The spatial variability of vehicle densities as determinant of urban network capacity. Philos. Trans. R. Soc. A Math. Phys. Eng. Sci. 368 (1928), 4627–4647.
Mirkin, B., Gutman, P.-O., Shtessel, Y., 2012. Coordinated decentralized sliding mode MRAC with control cost optimization for a class of nonlinear systems. J. Frankl. Inst. 349, 1364–1379.
Mirkin, B.M., 2003. Comments on “exact output tracking in decentralized adaptive control”. IEEE Trans. Automat. Control 48 (2), 348–350.
Mirkin, B.M., Gutman, P.O., 2003. Decentralized output-feedback MRAC of linear state delay systems. IEEE Trans. Automat. Control 48 (9), 1613–1619.
Mirkin, B.M., Gutman, P.-O., 2005. Output-feedback co-ordinated decentralized adaptive tracking: the case of mimo subsystems with delayed interconnections. Int. J. Adapt. Control Signal Process. 19, 639–660.
Olszewski, P., Fan, H.S.L., Tan, Y.-W., 1995. Area-wide traffic speed-flow model for the singapore CBD. Transp. Res. Part A 29A (4), 273–281.
Ortigosa, J., Menendez, M., Tapia, H., 2014. Study on the number and location of measurement points for an mfd perimeter control scheme: a case study of Zurich. EURO J. Transp. Logist. 3 (3–4), 245–266.
Ramezani, M., Haddad, J., Geroliminis, N., 2015. Dynamics of heterogeneity in urban networks: aggregated traffic modeling and hierarchical control. Transp. Res. Part B 74, 1–19.
Saberi, M., Mahmassani, H., 2012. Exploring properties of network-wide flow-density relations in a freeway network. Transportation Research Board 91st Annual Meeting. Washington, D.C.
Yildirimoglu, M., Geroliminis, N., 2014. Approximating dynamic equilibrium conditions with macroscopic fundamental diagrams. Transp. Res. Part B Methodol. 70, 186–200.
Yildirimoglu, M., Ramezani, M., Geroliminis, N., 2015. Equilibrium analysis and route guidance in large-scale networks with mfd dynamics. Transp. Res. Part C 59, 404–420.
Zhang, L., Garoni, T., de Gier, J., 2013. A comparative study of macroscopic fundamental diagrams of arterial road networks governed by adaptive traffic signal systems. Transp. Res. Part B 49, 1–23.
Zwart, H., Bontsema, J., 1997. An application driven guide through infinite-dimensional systems theory. In: Proceedings of the ECC97, Plenary Lectures and Mini-Courses, pp. 289–328.